CHARACTERISATION OF DOWNSHIFTING NANOPARTICLES

CLAUS CHRISTENSEN

Department of Physics and Astronomy
Aarhus University

August 2016

Claus Christensen: *Characterisation of Downshifting Nanoparticles*

SUPERVISOR:
Brian Julsgaard

LOCATION:
Aarhus

ABSTRACT

The global energy demand is increasing every year, and the fossil fuel resources are shrinking. Burning of fossil fuels also release greenhouse gasses which result in climate change. The need for a transition to renewable energy sources is larger than ever and solar energy has a huge potential due to the practically unlimited energy available from the sun.

Silicon solar cells account for the majority of the produced solar cells today. There is however limitations on their efficiency due to optical losses such as transmission of photons with energies below the silicon band gap at 1100 nm. A solution to transmission losses is upconversion, where two transmitted photons of low energy gets converted to one photon with an energy high enough to bridge the band gap in silicon. When using an erbium based upconverter, only a small fraction of the transmitted photons gets converted due to a narrow absorption range at 1500 nm to 1550 nm. A way to increase this absorption range, is to downshift all the photons between 1100 nm and 1500 nm to the erbium absorption range.

Downshifting nanoparticles (NPs) can do exactly that, and this study will focus on characterising commercially available PbS NPs for use in silicon solar cells. The NPs will be characterised by measuring absorption spectra and photoluminescence spectra while suspended in toluene as well as when deposited in PMMA thin films. Finally the quantum efficiency (QE) of the deposited NPs will be determined.

The characterisation shows good match between emission wavelength of the NPs in the toluene solution and the erbium absorption range. Once deposited in PMMA thin film the PbS NPs showed increased absorption, but a low QE in the order of 10^{-4}. Poor passivation is believed to be the cause for the low QE, but it was not ultimately decided whether the passivation was poor to begin with or was a result of the deposition method.

ACKNOWLEDGEMENTS

First, i would like to thank my supervisor Brian Julsgaard for guidance and support, and being available for helpful discussions.
Thanks to Harish Lakhotiya for introducing me to the spin coating technique, and the use of the Perkin-Elmer, and for always being willing to help when problems arose.
Thanks to Jeppe Christiansen for assistance in the PL lab.
Lastly a special thanks to Leon, for moral support during the long rainy summer days of writing this thesis, much appreciated.

CONTENTS

ACRONYMS

NP Nanoparticle

PbS Lead Sulfide

PL Photoluminescence

PLE Photoluminescence excitation

QE Quantum Efficiency

EQE External Quantum Efficiency

IQE Internal Quantum Efficiency

PMMA Poly(methyl methacrylate)

1 INTRODUCTION

The global energy demand increases every year, and fossil fuel resources are not unlimited. Climate changes are believed to be linked to the burning of fossil fuels through the release of greenhouse gasses. The need for clean renewable energy sources is growing fast and solar energy is one of the most promising candidates at the moment. Solar cells are used to harvest the practically unlimited amount of energy provided by the sun, and silicon solar cells is the most commonly used type with a market share of 90 % [10]. Silicon is one the most abundant elements in the earth's crust and non-toxic which makes it an attractive material for solar cells.

Silicon has an inherent limit to how much of the sun's energy it can convert though, due to its band gap of 1.12 eV. All photons with an energy below this threshold will be transmitted through the silicon and lost. To solve this issue, upconverters have been made that absorbs two photons with an energy below the band gap, and converts them into one photon with an energy that is above the silicon band gap. The problem with upconverters is their absorption range is fairly narrow. Erbium based upconverters absorbs mainly in the 1500 nm to 1550 nm range, whereas the silicon band gap is at 1100 nm. This still leaves a large range from 1100 nm to 1500 nm where the photons are not converted to electricity.

The solution to this is a fluorescent downshifting layer that absorbs light in the before mentioned range, and emits it at the upconverter absorption range. This combination of upconversion and dowshifting raises the theoretical limit of the silicon solar cell from 30 % to 40 % [24]. Downshifting nanoparticles (NPs) are a promising fluorescent material that can be tuned by varying the size of the particles, meaning they can be tailored to specific situations. They have already been studied in conjunction with solar cells, with the goal of downshifting the UV light from the sun to the visible region where silicon solar cells are more efficient [11, 19]. In this project the focus will be on NPs that can absorb in the 1100 nm to 1500 nm range and emit in the erbium upconverter absorption range.

The goal of this project is to characterise commercially available PbS NPs, implement them in a transparent host matrix and characterise their optical properties in the matrix. This will be used to determine whether the PbS NPs are a suitable candidate for use in silicon solar cells with an erbium upconverter. Part of the project is also to set up equipment for broad spectrum measurements. This includes a xenon lamp and monochromator that needs to be integrated in the ex-

isting laboratory set up and controlled from a computer via LabVIEW drivers.

Overall structure of the thesis: Chapter two is going to briefly explain the basics of a silicon solar cell and introduce the advanced upconverter system that consists of the upconverter and the fluorescent material. Chapter three will go over the theory behind the downshifting NPs, the quantum confinement effect that enables them to be tuned to specific emission wavelengths, and the aspect of surface passivation. Chapter four will introduce the experimental equipment used, among them the set up for PLE spectra that had to be implemented in the existing lab set up. Chapter five will be regarding the characterisation of the NPs as we acquire them, still in the toluene solution. Chapter six will go over the spin coating technique and the method used to deposit the NPs in a PMMA thin film on substrates. Chapter seven will be characterising these PbS in PMMA thin film samples, both structurally and optically. Chapter eight will be regarding the quantum efficiency measurements of the NPs, and will try to answer the question of whether the PbS NPs are suitable or not.

2 SILICON SOLAR CELLS

In this chapter the basics of a silicon solar cell will be presented and the different losses of energy occurring will be discussed. Thereafter the advanced upconverter system will be introduced, to reduce some of the inherent losses of the silicon solar cell.

2.1 BASICS OF A SILICON SOLAR CELL

Solar cells convert the radiation energy from the sun to electric energy, and do so by absorbing photons to generate a current. This works because silicon is a semiconductor and its energy levels are split into two bands, the valence band and the conduction band. Electrons in the valence band can absorb photons and gets excited from the valence band into the otherwise empty conduction band. This generates an electron-hole pair, where the hole is the now empty spot in the valence band where the electron used to be. The electron and the hole is then separated by an electric field caused by a pn-junction, and they move towards separate contacts placed on the surface of the solar cell, thereby causing a current. The energy required for a photon to be absorbed is determined by the band gap of the semiconductor. Silicon has a band gap energy of 1.12 eV which corresponds to about 1100nm. This means the minimum energy required for a photon to be absorbed is 1.12 eV since lower energy photons will not have enough energy to excite the electron up into the conduction band. It also means though, that photons with an energy higher than the band gap energy will not be converted efficiently. This is due to a relaxation process where electrons with energies higher than the conduction band minimum, will fall into energy states near the minimum of the conduction band, and the excess energy will be released as heat. This kind of energy loss is named thermalisation loss.

The other big energy loss in silicon solar cells comes from photons with energies below the band gap energy. These photons gets transmitted through the solar cell without being used. Spectral losses from thermalisation and sub band gap energy photons being transmitted can be as high as 50% for single junction silicon solar cells [21]. Figure 1 shows the solar spectrum along with the part that silicon solar cells can convert to electricity themselves. It also shows the thermalisation loss, as the blue part of the spectrum that is below 1100nm, and the transmission loss as the blue part above 1100nm. Due to these losses and others, the theoretical limit of a silicon solar cell is 30% [22].

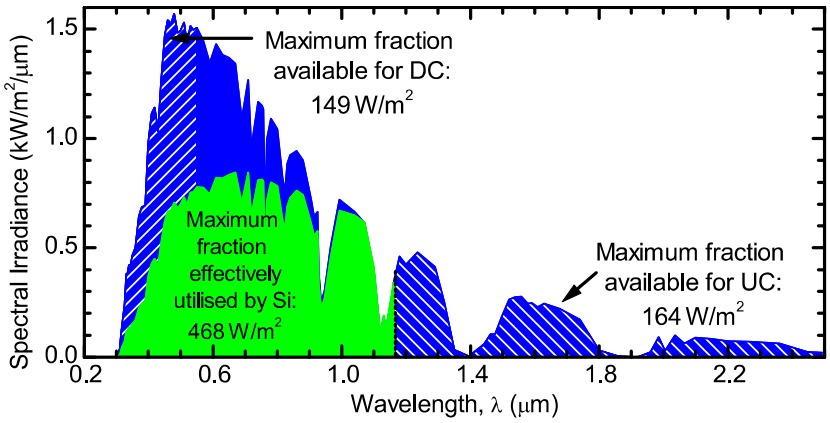

Figure 1: AM1.5G solar spectrum showing the part that can be converted to electricity by a silicon solar cell. From [18].

The different type of losses inherent to the silicon solar cell can be prevented by different kind of methods. The thermalisation loss in the UV and visible area can be prevented by downconversion for photons below 550 nm. Downconversion works by absorbing one high energy photon and emitting two low energy photons near the band gap energy where photons are most efficiently converted to electricity.

The other end of the spectrum, where the photons have lower energy than the band gap, requires upconversion to utilise the photons. Upconversion works by absorbing two low energy photons and emitting one high energy photon that has enough energy to excite an electron from the valence band to the conduction band. With an optimal upconverter the efficiency limit is raised to 40.2% for a silicon solar cell [24].

It is the photons in this region, specifically from 1100 nm to 1550 nm, that is the focus point of this study. In the next section, an advanced upconverter system will be discussed, that uses downshifting NP's in conjunction with upconverter material to upconvert the photons between 1100 nm and 1550 nm to photons with high enough energy to bridge the band gap of the silicon solar cell.

2.2 ADVANCED UPCONVERTER SYSTEM

The upconverter system described here was presented by J. C. Goldschmidt et. al. in 2008 [5]. The idea is to use the well known upconverter material $NaYF_4:Er^{3+}$ in which the erbium has conveniently spaced energy levels that allow for upconversion to silicon solar cells. The energy levels in erbium are positioned such that there is two evenly spaced excited states, which means two photons with the same energy can excite one electron to an excited state, and then the elec-

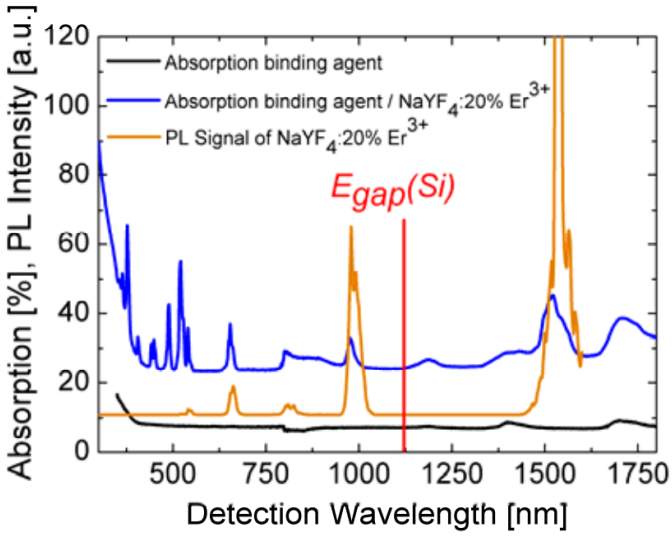

Figure 2: Absorption and luminescence spectra of $NaYF_4:Er^{3+}$. PL signal obtained with laser illumination at 1523 nm. From [5]

tron can fall back down to the ground state, emitting only one photon with the combined energy of the two absorbed photons.

The required energy of each of the first two photons is about 1500 nm to 1550 nm, which is far above the silicon band gap at 1100nm. The emitted photon has an energy of 800 nm if the electron drops directly down to the ground state, or 980 nm if the electron relaxes to an energy state just below before dropping to the ground state.

In Figure 2 is shown the absorption spectrum of $NaYF_4:Er^{3+}$ and the PL spectrum using 1523 nm illumination. It shows the absorption peak roughly between 1500 nm and 1550 nm and the resulting PL at 980 nm which is below the silicon band gap also indicated in the figure.

There is however one major issue with this upconverter, which is the narrow absorption range. It is only a small part of the transmitted photons above 1100 nm that gets upconverted to usable energies. The efficiency of the process is also dependent on the intensity of the light. The reason is that once the first photon is absorbed and the electron is in the first excited state, the second photon must excite the electron before it falls back into the ground state.

The solution to this problem is to introduce a fluorescent material that absorbs photons in the range between the silicon band gap at 1100 nm and the absorption in the upconverter at 1500 nm, and then emit in the absorption range of the upconverter. This is called downshifting. This spectral concentration will increase the amount of photons available for upconversion, from the narrow absorption range of the erbium upconverter, to the whole range from 1100 nm

to 1550 nm. It will also increase the efficiency of the upconverter, by increasing the intensity of the light in the absorption range, granting a larger chance for a second photon to be absorbed once the electron has been excited into the first excited state.

The proposed upconverter system including the fluorescent material is shown in Figure 3. It consists of the silicon solar cell on top and the fluorescent material in the bottom, with the upconverter layer in between. The figure also shows photonic structures between the fluorescent layer and the upconverter layer. These are needed since the fluorescent material also absorbs the photons emitted by the upconverter. The photonic structures work by reflecting photons in a specific range of wavelengths, and have been shown to improve the efficiency of fluorescent layers [6]. In this case they would need to reflect photons with energies above the silicon band gap, such as the photons emitted by the upconverter, coming from above. At the same time they should have high transmission for photons with energies below the silicon band gap, photons that need to be downshifted by the fluorescent material to the upconverter absorption range.

To achieve geometric concentration as well as the spectral concentration, the upconverter layer does not cover the whole backside of the solar cell. This means the fluorescent material collects light from the whole surface and concentrates it to the smaller upconverter surface, increasing the intensity on the upconverters, and thus their efficiency. To do this, photonic structures are needed between the fluorescent material and the areas not covered by upconverters, since we do not want the downshifted photons to exit the fluorescent material without going into an upconverter.

The fluorescent material is then to be chosen. Nanoparticles, nanocrystals, or quantum dots as they are also called, are a promising candidate because of their unique properties. They can be tuned to emit at a specific wavelength by varying their size. The next chapter will go over the theory of the NPs, explaining the quantum confinement effect which causes the emission wavelength to change when varying the size of the NPs.

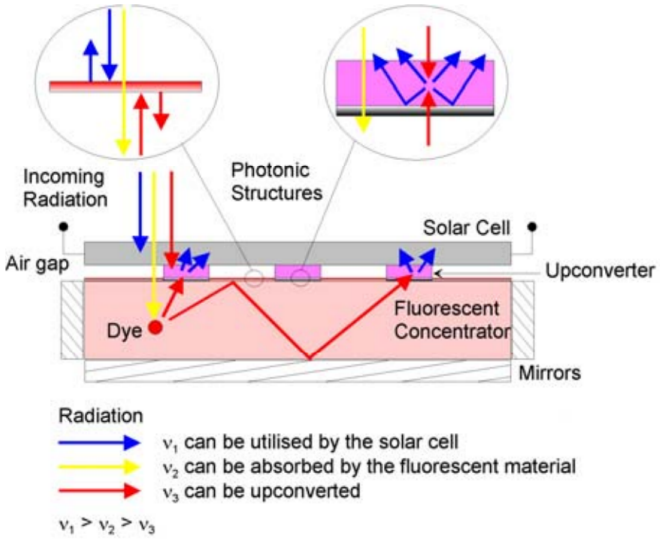

Figure 3: Advanced upconverter system as proposed by J. C. Goldschmidt et. al. [5]. Photons coming from the sun are split into three groups. The first group (ν_1) has energies above the silicon band gap and will be absorbed by the solar cell directly. The second group (ν_2) has energies between the silicon band gap and the upconverter absorption, and will pass through both the solar cell and the upconverter and then be absorbed by the fluorescent material which will downshift it to the absorption range of the upconverter (ν_3). This third group of photons (ν_3), coming from both the sun, and the florescent material, will then be absorbed by the upconverter and converted to higher energy photons (ν_1) that can be absorbed by the solar cell.

3 THEORY OF NANOPARTICLES

Semiconductor NPs has been studied extensively because of their unique optical properties. They are a means to probe the transition between bulk materials and molecules with their size often ranging from 1 nm to 10 nm. They are often used for their fluorescent properties, with a large absorption range and narrow emission peak that makes them ideal for downshifting. Probably the most important property of these NPs are their ability to be tuned to a specific emission wavelength, due to the quantum confinement effect which is described in the next section. This makes them a very interesting topic for use in solar cells. Solar cells are not equally efficient at all wavelengths as seen in the previous chapter, and downshifting NPs have been used for increasing solar cell efficiency in the the UV-Vis range. To do this the NPs are placed on top of the solar cell, and absorb short wavelength light that is poorly transformed by the solar cell, end emit it at higher wavelengths where the solar cell has a much higher efficiency [11, 16].

During synthesis of the NPs, their size can be controlled by varying different parts of the process, such as duration of reaction, temperature, and concentration of the different reactants [13, 27].

3.1 QUANTUM CONFINEMENT EFFECT

The quantum confinement effect, which is responsible for the NPs' ability to tune their emission wavelength, is a result of the NP diameter being of order of the Bohr exciton radius or smaller. In a bulk material the electrons are free to flow in all directions, and their energy spectrum is practically continuous. The density of states for the electrons will increase as the square root of energy, as seen in top part of Figure 4. If instead of being free to move in all directions, the electron is confined to a certain volume, it will gain kinetic energy which is called confinement energy in this case, and the energy spectrum of the electron becomes discrete. This is seen in the middle part of Figure 4.

NPs are are small enough to make the electrons feel confined, thereby going from the continuous bulk density of states, towards the discrete ideal QD density of states. The discrete energy spectrum also has an increased band gap, since the lowest energy state has a higher energy compared to the bulk energy spectrum. To get into the size range where the quantum confinement start having an effect, the size of the NP must be comparable to the size of the bound state of an electron-

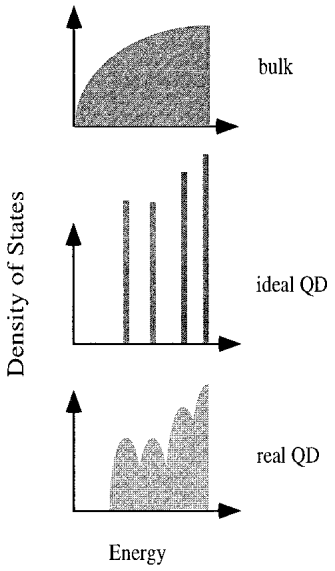

Figure 4: Density of electron states for bulk and size-quantised semiconductor. From [26]

hole pair, called an exciton. For PbS the Bohr exciton radius is 20 nm which makes the strong confinement region easily obtained [26]. Bulk PbS has a band gap energy of 0.41 eV which is a narrow band gap [25], and it allows for tuning in a large range that makes PbS suitable for a wide range of uses. NPs will not have perfectly discrete energy states, but rather something looking like the bottom part of Figure 4, due to size distributions. This still shows an increase in the band gap energy, and will also cause stronger absorption at certain photon energies.

A complete review of the electronic structure of PbS NP's will not be made here since it already exists in the literature. Wang et. al. [25] calculated the lowest exciton energies for PbS NPs using a parabolic effective mass model, and a hyperbolic band model. The hyperbolic band model proved far better at matching the experimental data, but is unable to calculate energies of higher excited states. Kang et. al. [12] used four band envelope function formalism to calculate the energies of the higher excited states, and the results agree well with measured properties of PbS NPs down to 3 nm in diameter. The 3 nm diameter NPs showed exciton energies of 2 eV, which is five times the band gap energy of bulk PbS, and proves the electronic states of the NPs are completely dominated by quantum confinement.

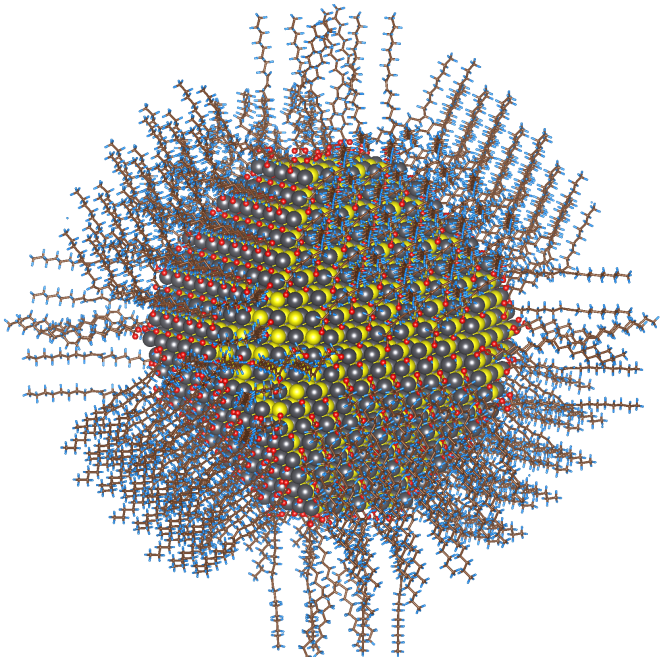

Figure 5: Calculated atomic structure of a 5nm diameter NP passivated with oleic acid. From [28]

3.2 SURFACE PASSIVATION

Silicon used in solar cells need some form of surface passivation to avoid surface recombination. In the same way, downshifting NPs need their surface passivated in order to avoid non-radiative recombination. At the surface of a NP, the crystal lattice is disrupted and surface atoms will not have as many bonds as the atoms in the middle that are surrounded by other atoms. The result is dangling bonds, which causes surface reconstruction and defects when the surface atoms find new equilibrium positions. These defects will introduce energy levels lying in the band gap of the semiconductor, between the valence band and the conduction band. The new levels in the band gap are called trap states and cause non-radiative recombination of an electron and a hole. This will reduce the quantum efficiency of the NP, since the absorbed photon will not cause a new photon to be emitted.

There are different ways of passivating the surface of NP's, but the general idea is to introduce a material that will attach itself to unbound atoms. This passivation layer stops the NP from reacting with the surroundings and prevents trap states.

One way is using an organic ligand such as oleic acid. The oleic acid will bind to the dangling bonds of the surface atoms, preventing them from introducing trap levels in the band gap. In Figure 5 is shown a

model of the calculated atomic structure of a PbS NP with a diameter of 5 nm. This model also shows the oleic acid ligands bound to the surface of the NP to passivate it. The oleic acid ligands also increase the solubility of the NPs in certain solvents while preventing agglomeration. The problem with the organic passivation using oleic acid, is that the ligands are large and bulky as seen in Figure 5. This makes it unlikely for the oleic acid to cover the entire surface of the NP due to steric effects, resulting in some trap states causing non-radiative recombination of electron-hole pairs[3]. In general, a significant fraction of organically passivated NPs show signs of surface related trap states that reduces the fluorescence quantum yield [17]. The long organic ligands also increases the inter-particle distance, reducing the absorption for a NP film of specific thickness.

A second way to passivate the surface is to grow an inorganic shell on top of the NP, consisting of another semiconducting material. This creates the so-called Core/Shell type NP. For optimal passivation the shell material should have a small lattice mismatch with the core surface. This reduces the amount of defects in the interface that can lead to trap states in the band gap. The shell material also needs to provide a sufficient potential barrier for photo excited electron-hole pairs generated in the core. These requirements are hard to meet with a single pure semiconductor and often an alloy material is used. For CdSe NPs an increase in the photo luminescence quantum yield from 9.2% to 89% was observed after growing a CdZnS shell on the NPs [3].

In general the surface passivation is an extremely important aspect of effective downshifting NPs. Their small size means the surface to volume ratio is very high, and surface trap states will greatly reduce the efficiency of the NPs by providing the electron-hole pairs with a non-radiative recombination, effectively wasting the absorbed photon.

4

EXPERIMENTAL SETUP

The experimental work is a big part of this thesis, and in this chapter i will introduce and describe the different characterisation techniques used. The equipment will also be introduced and and a short description of how they work.

4.1 PHOTOLUMINESCENCE MEASUREMENTS

The key aspect of the nanoparticles, is that they downshift light in the range between the silicon bandgap at 1100 nm, and the upconverter energy level around 1500 nm to 1550 nm. To effectively measure the downshifting in this range, broadspectrum illumination is needed. The existing setup in the laboratory only consisted of specific wavelength lasers and thus could not provide illumination to measure the downshifting in the entire range. As part of the project, equipment for broadspectrum measurements was to be integrated in the existing lab set up before any measurements could be done. In the next part the monochromator set up, consisting of a xenon lamp and the monochromator, will be described along with the detector. The integrating sphere used for quantum efficiency measurements will also be explained here. A manual for use of the monochromator has also been made and can be found in Appendix A. The purpose of this manual is a quick guide for new users of the monochromator.

Monochromator set up

The monochromator to be used is a Triax 180 from Jobin Yvon. It only goes up to 1400 nm while ideally we would want up to 1500 nm since the that is where the upconverter starts to absorb. It is a small gap though that is not believed to make a difference. The light spectrum from the sun as seen in Figure 1 also shows there is a gap near 1400 nm where little light actually reaches the surface of the earth due to absorption in the atmosphere caused by water molecules.

The light source is a xenon lamp in a box made to fit with the monochromator when placed next to each other. A power spectrum of the light coming from the monochromator set up is shown in Figure 6. The power meter used to measure this was specified to have an accuracy of 5 %, and the measurement was done at the sample holder.

When making the first measurements on the NPs using the monochromator set up, a rather strange set of peaks appeared in the measured spectra. At first it was just assumed to be the emission from the sam-

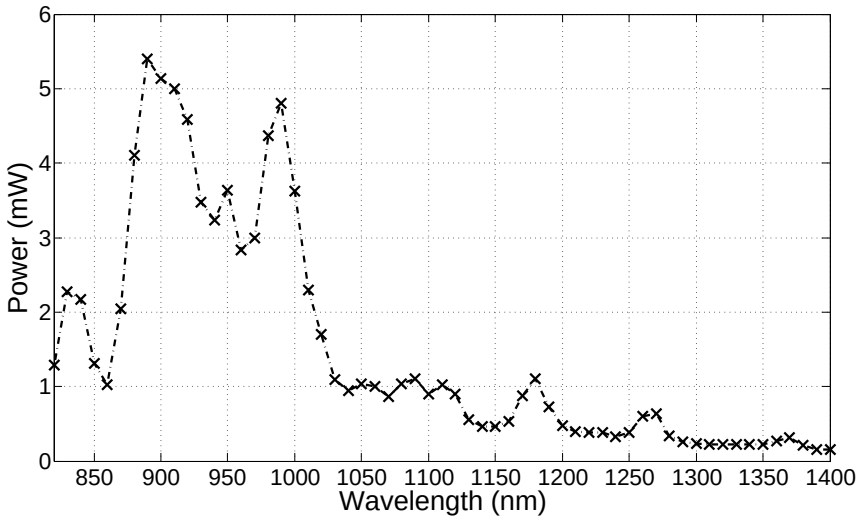

Figure 6: Power curve for light coming from the lamp + monochromator set up. The intensity was measured at the position of the sample holder, while using appropriate filters in front of the monochromator.

ples, however it was later revealed to originate from the monochromator. To get rid of this light that was in the same wavelength area as the light emitted from the NPs, short pass filters were acquired to mount in front of the monochromator, to eliminate higher order diffractions from coming out of the monochromator. The used short pass filters were 1200 nm, 1300 nm, 1400 nm, and 1500 nm. The 1200 nm filter was used for all excitation wavelengths below 1200 nm, then the 1300 nm short pass filter was used between 1200 nm and 1300 nm, and likewise for the 1400 nm and 1500 nm short pass filters. The monochromator does have a filter wheel of its own, with long pass filters installed. It has a 800 nm long lass filter which was used for all measurements along with the short pass filters mentioned. This combination eliminated leaking of unwanted light from the monochromator.

In Figure 7 is shown a spectrum of the light coming from the monochromator set up when set to 1300 nm. The actual position of the peak is at 1298 nm and this difference increases as the wavelength decreases. It is a very small discrepancy though, between the set wavelength and the actual wavelength. At 900 nm set wavelength the actual peak is at 890 nm while at 1400 nm it matches exactly.

The first thing the light passes through when leaving the monochromator is a concave lens to reduce the divergence of the beam. Two mirrors and a focusing lens then focuses and redirects the light to enter the beam path used by the lasers also present in the lab. A final focusing lens is placed just before the sample holder which focuses

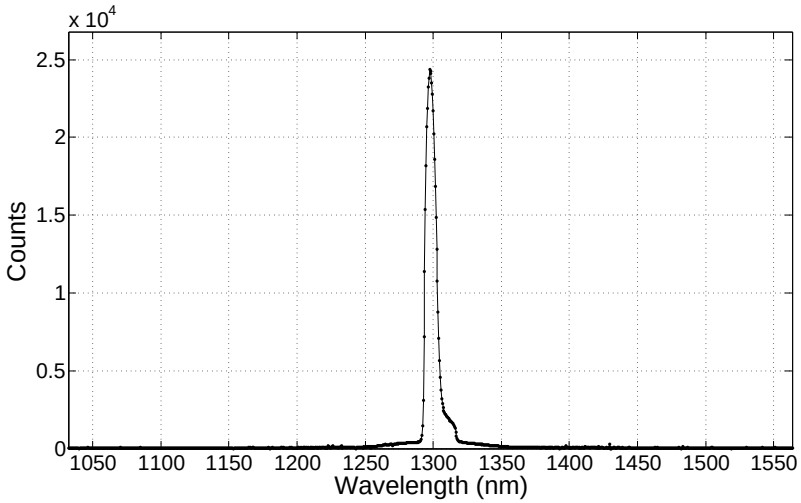

Figure 7: Example spectrum of the light coming from the monochromator set up at 1300 nm.

the beam to have a beam diameter of about 5 mm when reaching the sample holder. A large collection lens is placed to pick up the light coming from the sample and redirect it towards the detector.

Integrating Sphere

For making quantum efficiency measurements an integrating sphere is used. The sphere is hollow where the inside is coated with a diffusive reflective coating that reflect more than 99 % of incident light. The idea is that light hitting the surface is reflected and scattered uniformly, meaning that the light is distributed equally on all surfaces in the sphere. This will remove any non-uniform spatial distribution of the light inside the sphere.

When not using an integrating sphere, the detector is only measuring light emitted in the direction of the detector. When the sample instead is placed inside the sphere, light is collected from all emission directions, cancelling out any preferred emission direction the sample might have.

Detector

The detector used is a PyLoN-IR detector from Princeton Instruments. It is cooled with liquid nitrogen to -100 °C to reduce any thermal noise from the detector itself. Long pass filters were used in front of the detector to eliminate any of the excitation light from entering the

detector. Filters with a cut-off wavelength of 1200 nm, 1300 nm, 1400 nm, and 1500 nm were used. The 1200 nm long pass filter was used for excitation wavelengths below 1200 nm and the 1300 nm long pass filter was used for excitation light between 1200 nm and 1300 nm, and likewise for the rest.

Data collection was done with LightField software that controlled the detector. This program would control the integration length, averaging over several frames, and subtraction of a background spectrum from the measured spectrum. The maximum integration time was limited by the background noise. Even with the cooling to -100 °C the detector would be 50 % saturated at most wavelengths after only 1.5 seconds, just from thermal noise.

4.2 ABSORPTION MEASUREMENTS

For the NPs to be able to downshift the light, they need to absorb the photons, and the higher absorption they have the less NPs are needed to downshift the light. Absorption measurements are thus an important part in determining whether specific types of NPs are suitable for use in solar cells. Nano particles with high absorption would require a thinner layer, which would reduce material cost and make the cells cheaper.

To measure the absorption, a Perkin Elmer Lambda 1050 spectrophotometer is used. It can measure the transmission (T) and reflection (R) of a sample, and from that one can calculate the absorption (A). An example of such a measurement is shown in Figure 8 where a measurement on toluene has been done. It uses two beams, a sample beam and a reference beam. The sample beam goes through the sample and then its intensity is compared to the reference beam to see the transmission %. For measuring the reflected intensity, the sample is placed behind the detector which then measures the intensity of the light being reflected from the sample. When you have transmission and reflection, absorption is a simple calculation,

$$A = 1 - T - R$$

Before making any measurements, the beam intensities have to be adjusted. The sample and reference beam should have the same intensity for accurate transmission and reflection measurements. First the detector gain is adjusted until the sample beam intensity lies between 80 % and 90 % of saturation power. Then the reference beam intensity is adjusted by changing the size of the beam using an aperture, until the intensity is the same as that of the sample beam. Then you make the first measurement, which is always a baseline (100 % transmission) measurement, by removing any sample from the sample compartment, and choosing scan range and speed. The measure-

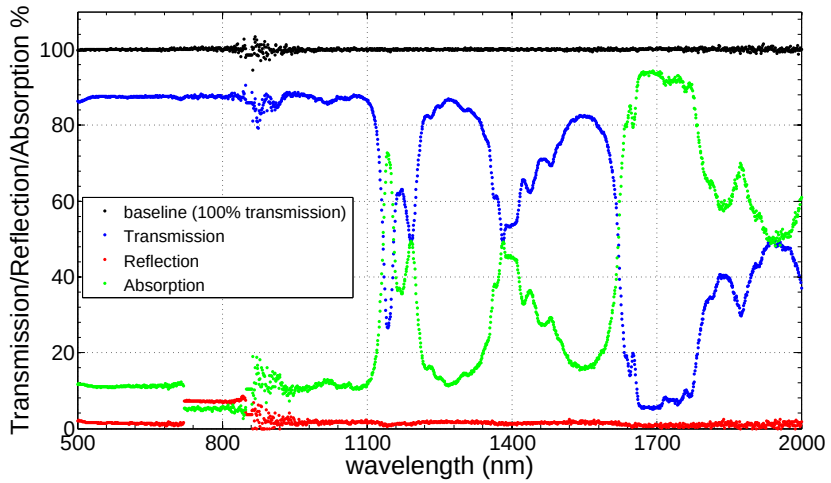

Figure 8: Example of a measurement on toluene with the Perkin-Elmer spectrophotometer.

ment starts at the highest wavelength in the range, and then scans towards the lowest wavelength.

4.3 PROFILOMETRY MEASUREMENTS

A profilometer is as the name suggests, an instrument for measuring the profile of a sample. This can be used to measure the roughness of a surface or the thickness of a film deposited on the surface of a substrate. The Bruker DektakXT stylus profiler is a contact method profiler, meaning it uses a stylus that touches, and is moved across, the surface of a sample. The vertical displacement of the stylus as it moves across the sample, will generate an analog signal that is converted to a digital signal which is processed and displayed on a computer. The scanning speed and length is chosen beforehand on the computer, along with other settings such as measuring range and stylus size. For measuring film thickness, a scratch has to be made in the sample that the stylus will move across. When making the scratch, it has to be done using something that will cut through the film, but not scratch the substrate below the film. In Figure 9 is shown an example of a profilometer measurement, which also shows what typically happens when making the scratch, namely that the film matter is pushed to the side and shows up as peaks next to the scratch groove. This is then taken into account when setting the zero point line to represent the surface of the film to accurately measure the thickness of the film.

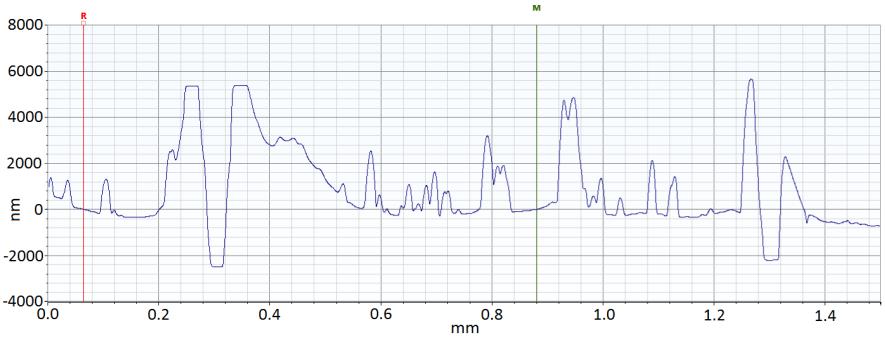

Figure 9: Example of a profilometry measurement. It shows two scratches made in the film, and the film material that is pushed to the sides and up, next to the scratches.

4.4 SEM IMAGING

When trying to gain an understanding of things that are new to us, a good starting point is having a look at it. There are different ways of doing this, and they each have their own advantages and drawbacks. The general notion is that the more detailed an image is, the more information can be gained from it. When working with physics on nano-scale, using your eyes to examine things does not work so well since the wavelength of the light our eyes can perceive is longer than the scale of what we are trying to look at. This means we have to use other methods for creating an image. An often and easily used method is Scanning Electron Microscopy (SEM) which uses electrons instead of photons to create an image of a sample.

SEM works by scanning the sample with a beam of electrons. The electron beam is moved across the sample one line at a time to generate an image. The speed at which the beam scans the sample can be varied and a slower scan will give a better image with more details. A diagram showing the components of a SEM is shown in figure 10. The electrons used used in the beam comes from the electron source at the top of the microscope. A negative voltage is applied to the electron source which causes electron to detach and accelerate towards the anode which is positively charged compared to the electron source. Some of the electrons will accelerate right by the anode, down towards the sample. Next the electrons will pass by magnetic lenses that will concentrate and control the focus point of the beam, with a goal of creating a small spot size on the sample. The scanning coils are responsible for scanning the beam across the sample as their name suggests.

Once the electrons hits the surface, they interact with the sample in different ways giving different signals. One way of interaction is elastic scattering which sends the incident electron back out again, transferring little or no energy at all. These are called backscatter electrons and there is a specific detector in place to detect these. This detector is

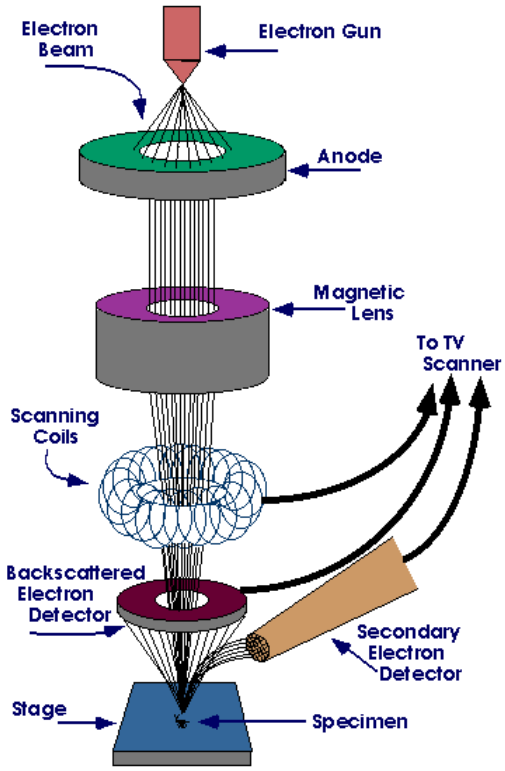

Figure 10: Diagram showing the different components of a scanning electron microscope and how they work together. From [1].

placed around the incoming electron beam since the backscatter electrons are mostly reflected back in the same direction from where they came. Another interaction is inelastic scattering which occurs when the incident electrons transfer some of their energy to electrons in the sample, which are then detached. These detached electrons from the sample are denoted secondary electrons and have energies less than 50 eV. Due to the low energy of these electrons, only electrons originating from within a few nanometres of the sample surface will completely detach from the sample and be able to reach the secondary electron detector [7]. Since the secondary electron detector is placed to the side of the sample, a small grid is placed in front of the detector and carries a positive voltage to attract the secondary electrons. The voltage on this grid is chosen so it attracts the low energy secondary electrons but not the higher energy backscattered electrons, and is typically around 250 V. Due to the secondary electrons originating from only the surface of the sample, they are the optimal detection choice for creating images of the surface topography, while backscatter electron detection is more often used to detect areas with different chemical composition.

5 CHARACTERISATION OF PBS IN TOLUENE

The goal of this study, as with so many others, is to improve the efficiency of the solar cell. The increased efficiency is however not worth much if the cost of improvement, exceeds the benefits gained from the increased efficiency. This means the focus is also on making the improvements cost effective. For this reason among others, the downshifting NPs used should be commercially available. The chosen NPs are PbS NPs manufactured by Sigma Aldrich and have an advertised nominal emission wavelength of 1600 nm. They are available in 200 nm intervals, so the choice was between 1400 nm and 1600 nm. The 1600 nm was chosen for its closer proximity to the 1500 nm to 1550 nm upconverter absorption range.

The NPs arrive in a toluene solution with a concentration of 10 mg/mL. They are said to be colloidal NPs, which means they are suspended in the toluene solution while remaining evenly distributed. The toluene solution is completely black indicating high absorption in the visible range as expected.

This chapter will describe the characterisation process of the NPs while still in the toluene solution. The first measurements made on the NPs was absorption and emission spectra, to characterise their downshifting capabilities. Later chapters will be concerning the deposition of the NPs onto substrates, characterising the result, and observing any effects the deposition has on the optical properties.

5.1 ABSORPTION MEASUREMENTS

Measuring the absorption of PbS NPs in toluene was done using the Perkin-Elmer Lambda 1050 spectrophotometer which is described in chapter 4.2. The goal is to get the relationship between the absorption coefficient and the wavelength of the light incident on the NPs.

A quartz cuvette with a path length of 10 mm was used to hold the PbS in toluene solution during the measurement. Besides measuring the transmission and reflectance of the PbS in toluene solution, a cuvette with only toluene in it was also measured. This is needed since we can not extract the PbS NPs from the toluene solution and only measure the absorption on them. So when measuring the absorption of the PbS in toluene solution, we actually measure the combined absorption of PbS and toluene, but when also measuring the absorption of toluene alone, the PbS absorption coefficient can be isolated and calculated.

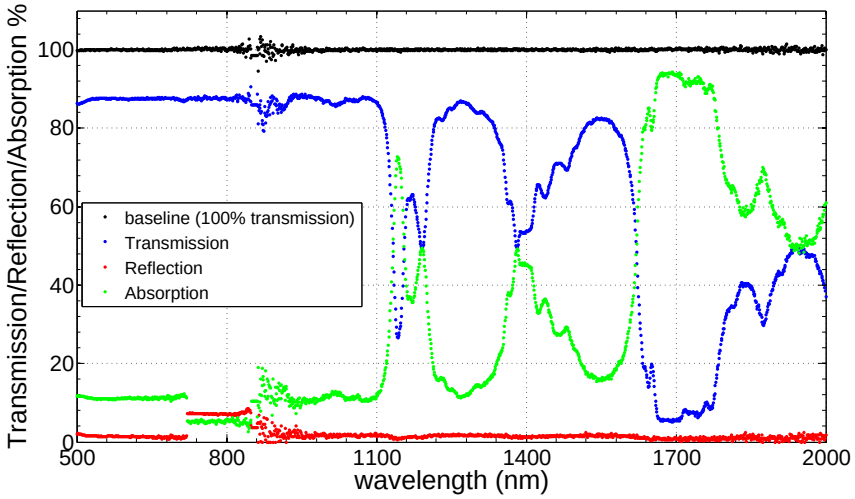

Figure 11: Transmission and reflection measurement of toluene. The absorption curve is calculated by subtracting the transmission and reflection from the baseline.

First off the transmission (T) and reflection (R) of a cuvette containing only toluene is measured. These two can then be used to calculate the absorption (A)

$$A = 1 - T - R \tag{1}$$

The result of this measurement can be seen in Figure 11. There are a few effects inherent to the Lambda 1050 spectrophotometer that is seen in the figure. The first thing to notice is the jitter around 860 nm that occurs on all four curves. This is caused by the change of detector by the spectrophotometer, and can not be avoided. The second thing that seems odd, is the reflection curve that has a sudden jump around 800 nm, which in turn causes the absorption curve to experience a sudden dip in the same range. No explanation was found for this behaviour, and happened several times in consecutive measurement, with varying jump size in the reflection. The data shown is the measurement with the lowest jump. Due to the placement of the jump, starting near the detector change, it is believed to be related to that and not a sudden higher reflection of toluene in this range.

Next up transmission and reflection measurements were done on a cuvette containing the PbS in toluene solution. At first a measurement was done with the original PbS concentration of 10 mg/mL, this proved to be too much though, as it showed practically 100 % absorption in almost the entire range. To solve this problem a new solution was made where additional toluene was added to dilute the PbS concentration. The new solution consisted of 1 part 10 mg/mL PbS in toluene solution, and 9 parts toluene, bringing the new solution to a 1 mg/mL PbS concentration. The result of this measurement can be seen in Figure 12.

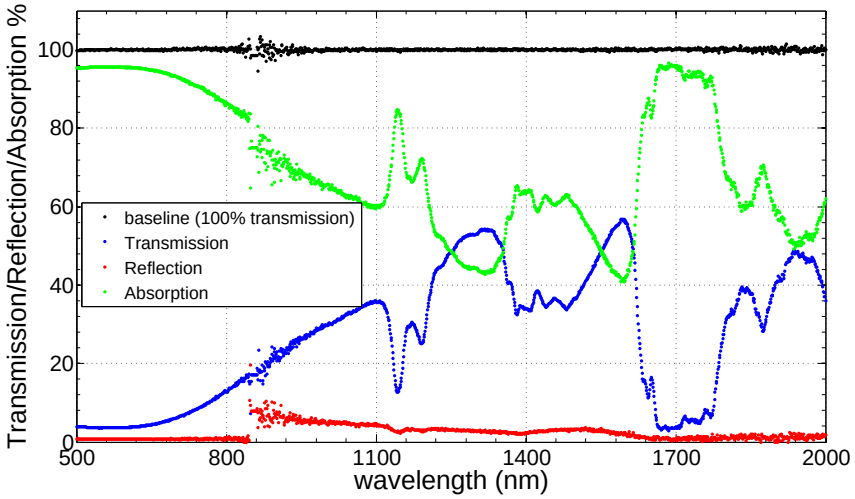

Figure 12: Transmission and reflection measurement of PbS in a toluene solution. The absorption curve is calculated by subtracting the transmission and reflection from the baseline.

The transmission and absorption in Figure 12 is vastly different from that of the toluene measurement, specially at shorter wavelengths where much higher absorption is occurring. In the other end of the spectrum, specifically above 1600 nm, there is nearly no change in the transmission spectrum. This general behaviour is quite as expected since the PbS NPs were advertised as having an emission wavelength of 1600 nm. This means their band gap is at 1600 nm and thus can not absorb light with longer wavelengths. We now have all the data needed to calculate the absorption coefficient for the PbS NPs.

5.1.1 *Absorption coefficient*

The absorption coefficient is a measure of how much light is absorbed by a material, as the light travels through it, and it has units of inverse length. In Figure 13 is shown a simple diagram that shows a box of length L with some kind of particles in it. Light enters the box from the left with a specific intensity I_{in} and leaves the box with another intensity I_{out}. This outgoing intensity can be calculated if you know the length of the box and the absorption coefficient (a) of the particles in the box using

$$I_{out} = I_{in} \cdot e^{-La} \tag{2}$$

On the other hand, when making absorption measurements you normally do not know the absorption coefficient, but instead measure the incoming and outgoing light intensities through a container with

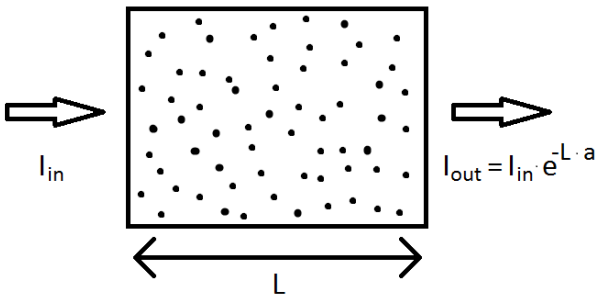

Figure 13: Simple diagram showing how the absorption coefficient a is calculated based on the incoming and outgoing intensities.

known length L. The absorption coefficient can then be isolated in equation 2 and you get

$$a = (\ln(I_{in}) - \ln(I_{out}))\, L^{-1} \tag{3}$$

In our case, the absorption in the PbS solution is a combination of absorption in both the PbS NPs, and the toluene. This means the absorption coefficient a in equation 2 should be replaced with $a_{toluene}$ and a_{PbS} like so

$$I_{out} = I_{in} \cdot e^{-L(a_{toluene} + a_{PbS})}, \tag{4}$$

and similarly in equation 3.

This is why it was also needed to make a measurement with only toluene in the cuvette to get the toluene absorption coefficient, and this leaves only the PbS absorption coefficient unknown for the PbS solution measurement. To do this though, it is assumed that the toluene absorption is the same in both cases. This was deemed a fair assumption since the concentration of PbS was only 1 mg/mL and thus barely even changed the toluene concentration.

The measured absorption coefficient for the PbS NPs while in a toluene solution is shown in Figure 14. The general trend of high absorption at lower wavelengths and lower absorption at higher wavelengths agrees with what we saw in the two transmission measurements shown in Figure 11 and 12. There is also the jitter around 860 nm that is caused by the changing of detector as seen previously. Then there is the small dip at 1150 nm and the odd looking peaks from 1650-1780 nm. These two features both happen in areas with very high toluene absorption and thus is not considered an inherent attribute of the NPs, but rather an effect causes by very high overall absorption in the cuvette.

The first 150 nm of the absorption curve is not believed to be the real value, since in this range there was almost 100 % absorption. This

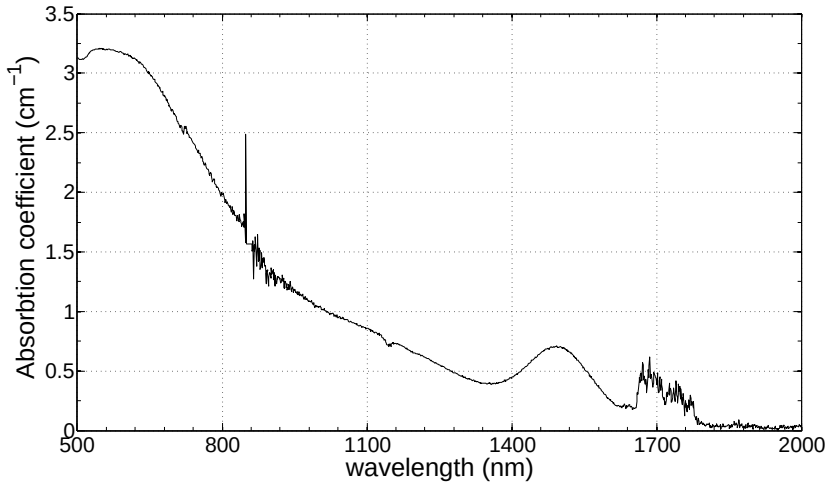

Figure 14: Absorption coefficient of PbS NPs while in a toluene solution.

means the value shown in the graph is just a lower bound and the real value is believed to continue to rise down towards 500 nm. This is backed up by [9] and [2] which also show an increase in absorption coefficient for decreasing wavelengths below 800 nm.

A feature that is not so easy to spot from previous measurements is the peak centered at 1495 nm. Since the absorption drops to almost zero right after the peak, it must be the excitation of electrons from the valence band, to the bottom of the conduction, and thus the minimum photon energy required to be absorbed. The shape of the absorption curve shows us the first excited state at 1495 nm, but also has a hint of a second excited state around 1100 nm, in the form of a small bump on the curve. The second excited state is even more clear in [2, 9, 20].

The absorption coefficient curve is very smooth, compared to the two absorption curves for toluene and the PbS in toluene solution. The two absorption curves are shown together in Figure 15. Despite the many spikes in the spectrum they are still producing a smooth absorption coefficient.

As we shall see in chapter 7.1 the average diameter of the NPs is roughly 7.3 nm and they appear spherical in shape. This info, along with a PbS density of 7.6 g/cm^3, and a 1 mg/mL concentration in the diluted toluene solution, allows us to calculate the particle concentration to $6.5 \cdot 10^{14}$ particles per mL. Now the cross section can be calculated using

$$\sigma = \frac{a}{n} \tag{5}$$

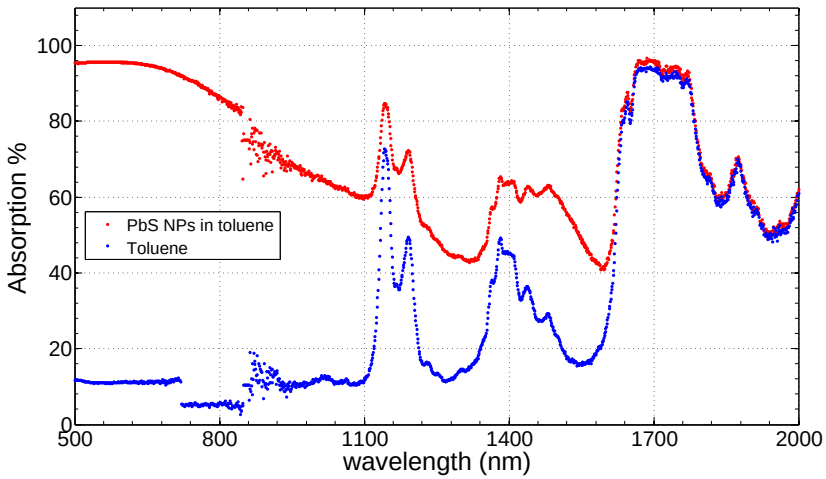

Figure 15: A comparison between the absorption spectrum of toluene and PbS in toluene.

where σ is the cross section, α is the absorption coefficient, and n is the particle concentration. The cross section curve is exactly the same shape as the absorption coefficient shown in Figure 14. At 800 nm this gives a cross section of $3.1 \cdot 10^{-15}$ cm^2, and at 1500 nm it is $1.1 \cdot 10^{-15}$ cm^2.

As we shall see in the next section, the absorption peak at 1495 nm is a slightly higher energy than the emission peak, and the reason for that is the stokes shift that is occurring. When an electron is excited by a photon and gets up in the conduction band, it will quickly drop down to the bottom of the conduction band. This is called relaxation and the extra energy is dissipated in the lattice as heat. When the electron then drops to the valence band from the conduction band, it releases a photon with slightly less energy than it absorbed.

5.2 PHOTOLUMINESCENCE MEASUREMENTS

The photoluminescence (PL) measurements were done using the equipment and set up described in chapter 4.1. The goal of these measurements is to see the downshifting effect of the NPs and specially their emission wavelength which is advertised to be 1600 nm. The desired wavelength however is between 1500 nm and 1550 nm where erbium upconverters have their upconversion absorption peak.

Some small changes in the set up was required to accommodate measuring on a liquid in a cuvette. The usual sample holder made

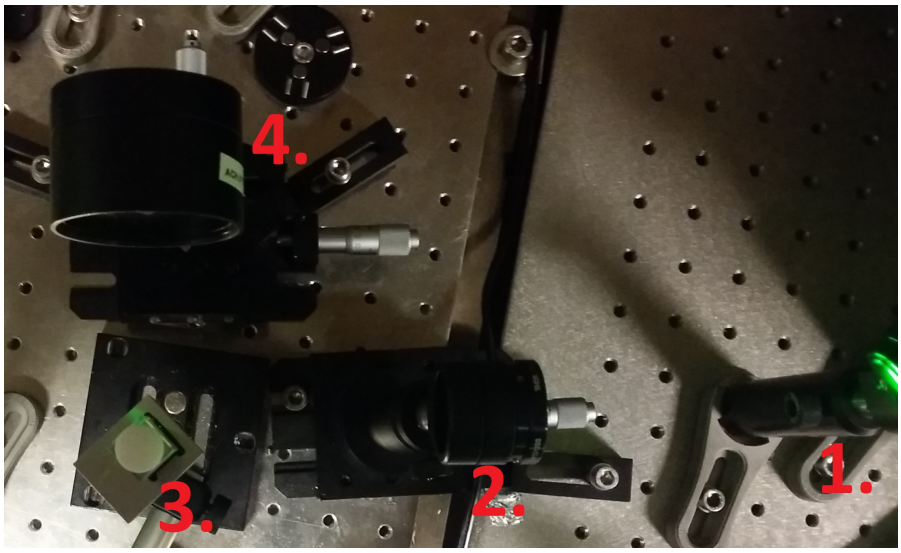

Figure 16: Sample holder set up for measurements on PbS in toluene. Light comes in from the right where a mirror at position 1 redirects it to go through a focussing lens at position 2 before it hits the cuvette at position 3. Lastly a collection lens at position 4 will collect some of the light emitted from the NPs and direct it towards the detector.

for solid samples, usually on silicon or quartz, was replaced with a special holder for the cuvette. A top down view of the cuvette holder placement is seen in Figure 16 where it is located in the bottom left. The light comes in from the right side, goes through a focussing lens, and hits the cuvette. A collection lens placed in the top left of the picture will collect some of the light emitted from the NPs and direct it towards the detector.

The first time making PL measurements on PbS in the toluene solution, a plastic cuvette was used. This turned out to be less than optimal since it was partly dissolved by the toluene. Later a quartz cuvette was acquired and the measurements done again which yielded quite a different result. Results will be shown for both cases starting with the plastic cuvette.

A measurement series was made using excitation light from 800 nm to 1400 nm in increments of 10 nm. The integration time was 1.5 s, and for each excitation wavelength the measurement was done 10 times and then the average was used as the final spectrum. Before the measurement series, the adjustable lenses and mirrors were optimized for highest detector signal, and the same setting was used for all wavelengths in that series. Slit width of the detector was 200 µm.

An example of an emission spectrum can be seen in Figure 17 where it is shown for 1000 nm excitation light. This shows a peak emission wavelength of approximately 1620 nm. The peak emission wavelength did have a small dependency on excitation wavelength

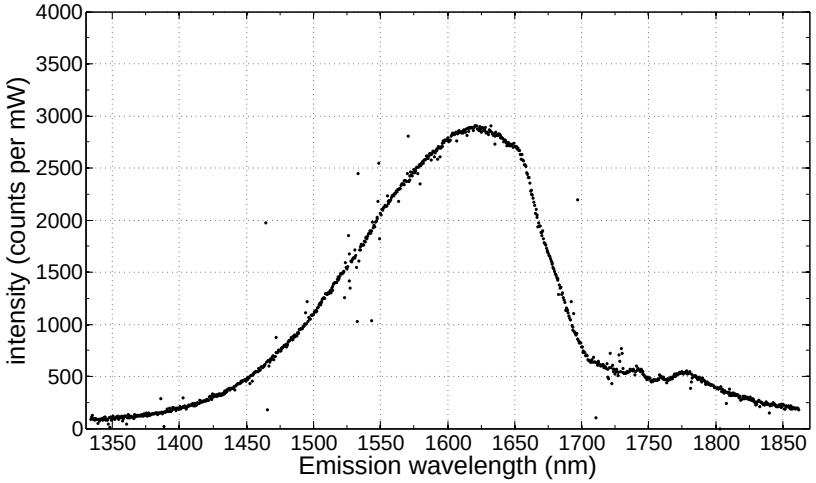

Figure 17: Emission spectrum of PbS NPs in toluene solution in a plastic cuvette, using 1000 nm excitation light.

since it varied from about 1615 nm at 800 nm excitation wavelength, to 1630 nm at 1400 nm excitation wavelength. The peak is very asymmetric, and the explanation for that can be found in the absorption spectrum for toluene shown in Figure 11. Toluene has very high absorption in the range from 1650 nm to 1770 nm, which means photons emitted from the PbS NPs in this range has a high chance of getting absorbed by the toluene. This explains it nicely since the emission peak is only asymmetric in the exact same range where toluene has high absorption.

Using the series of PL measurements, photoluminescence excitation (PLE) spectres were made. A PLE spectrum consist of data at a specific emission wavelength, for all excitation wavelengths. In Figure 18 is shown the PLE spectrum for PbS NPs in toluene solution at 1620 nm emission wavelength. Each data point is calculated by integration over the corresponding emission spectrum from 1615 nm to 1625 nm. The result is this almost linear increasing curve. This is not quite what was expected based on the absorption measurements shown above. PLE spectres is often used to find absorption peaks, and thus should generally follow the shape of the absorption coefficient. This is far from the case here since as we saw in Figure 14 the absorption coefficient decreases in the range from 800 nm to 1400 nm. The explanation could be that the emission spectres are normalised with regards to the power of the light hitting the sample, instead of the amount of photons hitting the sample. This causes an increase in

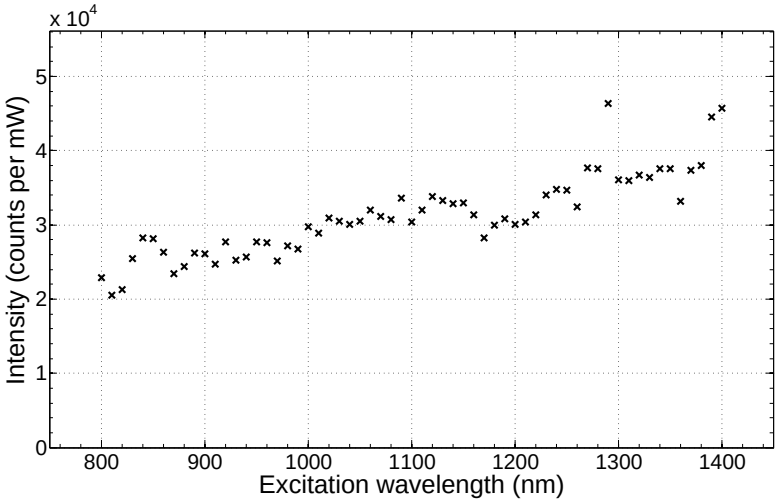

Figure 18: PLE spectrum for PbS NPs in toluene solution in a plastic cuvette at 1620 nm emission wavelength. Normalised to the power of the light hitting the sample.

the PLE spectrum since it takes an increasing amount of photons to have the same power at increasing wavelengths.

In Figure 19 is shown the same PLE spectrum at 1620 nm emission wavelength, but this time normalised for amount of photons hitting the sample. The curve is now nearly flat which means we get the same ratio of emitted photons to incident photons at all wavelengths. Since we know that the absorption coefficient is not constant in this wavelength range, it could indicate that all the light gets absorbed in the cuvette. This does seem very plausible if we look at the absorption coefficient, which is at roughly 0.5 cm^{-1} at the lowest point in the 800 nm to 1400 nm range for a diluted solution with one tenth of the PbS NP concentration. This gives a penetration depth of 2 mm for the PbS solution used for the PL spectres. Even though the light is not hitting the cuvette straight on but at an angle, as seen in Figure 16, the cuvettes dimensions are 10 mm x 10 mm which means the light path through it is several times longer than the penetration depth. This could explain the PLE spectrum, that for higher wavelength with lower absorption, the light just gets absorbed deeper in the cuvette.

As mentioned in the beginning of this section the plastic cuvette used was partly dissolved by the toluene, and later a quartz cuvette was acquired and the measurement done again. The PL spectrum for 1000 nm excitation light is shown in Figure 20. The big thing to

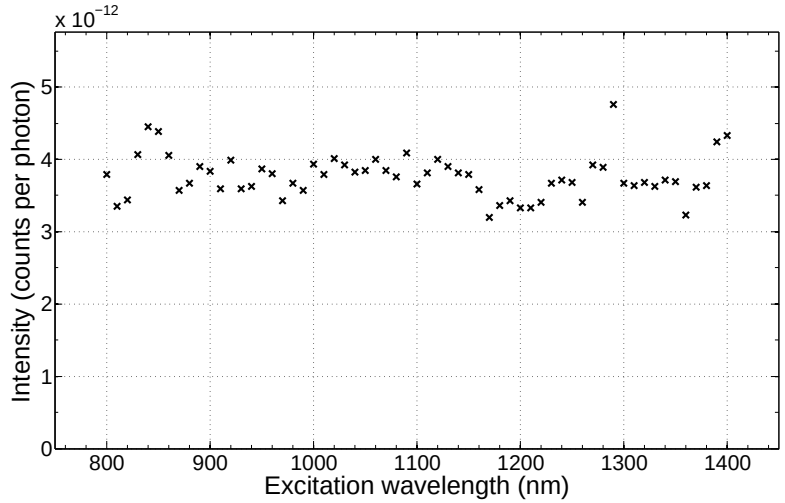

Figure 19: PLE spectrum for PbS NPs in toluene solution in a plastic cuvette at 1620 nm emission wavelength. Normalised to the amount of photons hitting the sample.

notice is the peak is now located just below 1550 nm, a substantial difference from the 1620 nm seen above. The cause of this change must lie with the dissolved plastic cuvette, where it must have mixed with the PbS NPs in the toluene solution. It is not fully understood how it affected the NPs, but if we look at the electrons as particles in a potential well, their energy levels are dependent on the depth of the well, and the thickness of the sides. When the dissolved plastic mixed with the PbS NPs, it would change the surroundings of the NPs and thus the surroundings of the potential well. This could either decrease the depth or make the walls thinner, and thus decrease the energy levels. This reduces the band gap and thus the energy of the emitted photons.

On the right side of the peak one can see the absorption in toluene starting at 1650 nm where the curve drops quickly instead of mirroring the other side of the peak, just as was seen in Figure 17. The full width at half maximum (FWHM) is about 95 meV for this peak, which is about the same as the 100 meV measured in [9] for PbS NPs with a diameter of 6.5 nm. They report a fairly narrow size dispersion of 10-15 % which it would seem is about the same for the PbS NPs used in this project based on the width of the emission peak.

A PLE spectrum was also made and can be seen in Figure 21. This is again normalised to the amount of photons hitting the sample. This looks very different compared to the PLE spectrum for PbS in the

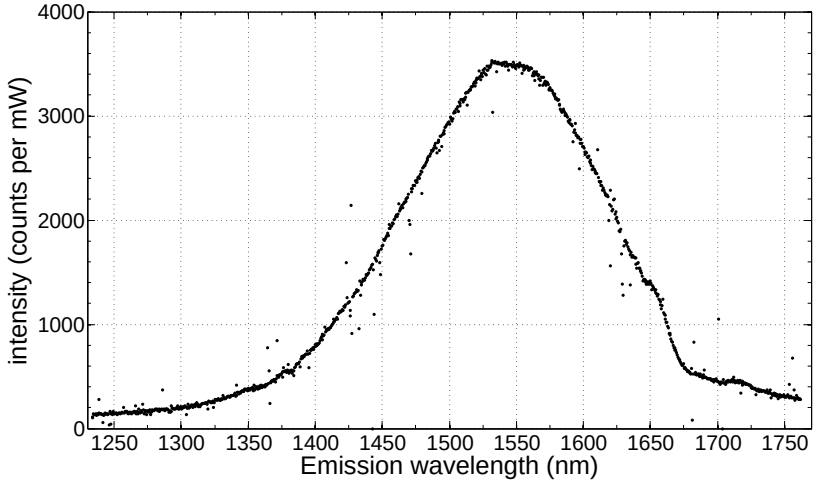

Figure 20: Emission spectrum of PbS NPs in toluene solution in a quartz cuvette, using 1000 nm excitation light.

plastic cuvette. We see a decrease in emission for longer wavelengths, just as one would expect according to the absorption coefficient, but a fairly flat curve in first half of the PLE spectrum. This could indicate a specific length of the light path through the cuvette, one where light below approximately 1200 nm would be almost completely absorbed due to the higher absorption coefficient, while light above 1200 nm would partly pass through the cuvette because of the low absorption coefficient for higher wavelengths. The problem with this explanation though, is that the penetration depth is much shorter than the dimensions of the cuvette, so even at higher wavelength where the penetration depth is largest, it is still several times shorter than the width of the cuvette.

A possible explanation could be concerning the ability, of the light emitted by the NPs, to exit the cuvette. As mentioned before the penetration depth is larger for higher wavelength, which means the NPs that absorb the light is positioned deeper into the cuvette. This means that for higher excitation wavelength, the emitted light has a longer path to travel before it exits the cuvette. A longer path means higher chance for it to be absorbed by toluene, or even absorbed by other PbS NPs. The toluene absorption curve shown in Figure 11 also shows increased absorption in the 1200 nm to 1400 nm range, the same range where the excitation spectrum is decreasing. The reason this is not seen in the case with the plastic cuvette, it that it was shaped slightly different. While the quartz cuvette is square, the plastic one had a more narrow light path through, meaning there was a shorter path length from the toluene solution, and out of the cuvette.

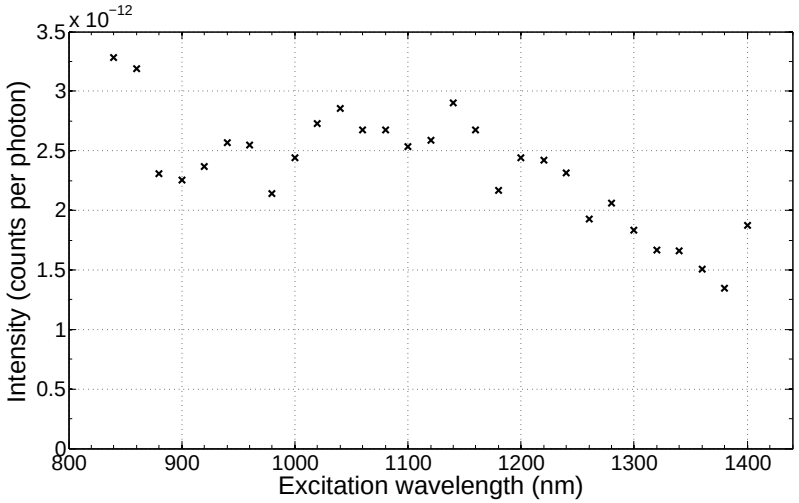

Figure 21: PLE spectrum for PbS NPs in toluene solution in a quartz cuvette at 1550 nm emission wavelength. Normalised to the amount of photons hitting the sample.

Regarding the results for the measurements made with the plastic cuvette, it is clear that the dissolved plastic mixed with toluene and PbS NPs had some effect on the properties of the NPs, but it will not be further investigated.

Now we have both the absorption and emission of our PbS NPs in toluene solution, and they are shown together in Figure 22. The PL spectrum shown is taken at 1000 nm excitation light while in a quartz cuvette. From this we can see the stokes shift is about 50 nm which is similar to what was found by Hines et al. [9]. The shape and width of the absorption and emission peak also match each other very well as expected. The fact that they are in a toluene solution can be seen on both curves from 1650 nm to 1770 nm where toluene has very high absorption.

Figure 22 shows very well the downshifting properties of the NPs, in the way that they absorb light in a large range mainly below 1600 nm and then emit in a relatively narrow range between 1400 nm and 1700 nm. Since the range of interest for emission is 1500 nm to 1550 nm for the upconversion, there is still adjustments needed for optimal emission wavelength.

The next two chapters will be regarding the deposition of the NPs onto substrates using spin coating, and the characterisation of the resulting samples, including structural and optical characterisation.

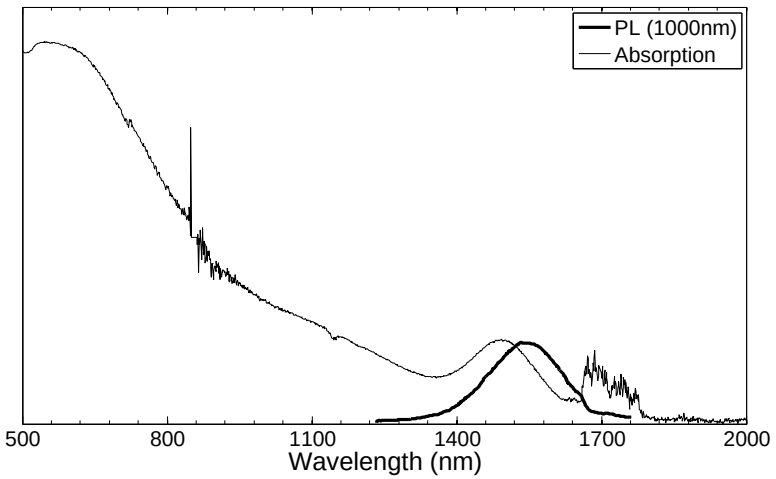

Figure 22: Absorption (thin line) and PL (bold line) for PbS NPs in toluene solution. The PL spectrum is taken at 1000 nm excitation light. Y-axis units are arbitrary and the PL spectrum has been scaled to match the absorption peak at 1500 nm.

6

MAKING SAMPLES USING SPIN COATING

The next step in the process of characterising the PbS NPs is to deposit them on substrates to see how it affects their properties. This is a crucial part since they have to be deposited in a film on a substrate before they can be implemented in a solar cell. As we just saw in the previous chapter, changing the environment of the NPs can alter their properties such as emission wavelength. This is not necessarily a bad thing however, as the optimal emission wavelength for downshifting NPs in the advanced upconverter system described in section 2.2 is 1500 nm to 1550 nm.

This chapter will describe the general technique of spin coating and and the process i followed, including the cleaning of the substrates prior to spin coating the thin film onto them.

6.1 SPIN COATING

Spin coating as a method has been used for many decades for the application of thin films to substrates with a flat surface. The process is fairly simple and a diagram showcasing the different steps taking place, is shown in Figure 23. It starts with placing a small puddle of the solution at the center of the substrate. Next step is rotating the substrate at high speed to spread out the coating material evenly across the substrate. The centrifugal force is what causes the material to spread out and is proportional to the spinning speed. Often the spinning process is split into two parts, where the first part is done at relatively low speed of maybe 1000 rpm for 10 seconds. This slow spin part is done to make sure the solution is spread out and covering to entire substrate surface, before the last high speed part where the film thickness is defined. Most of the solution placed on the substrate will end up being wasted due to being thrown off the substrate. This will leave a thin homogenous film on the surface of the substrate. The last step is heating the sample to evaporate any left over solvent still in the film. This will increase the physical stability of the film before handling the sample.

The thickness of the resulting film depends on several parameters such as spinning speed, spinning time, and viscosity of the fluid, with the most important one being spinning speed. The speed determines the centrifugal force applied to the solution on the substrate. The solution will continue to spread out during spinning, while simultaneously drying due to the solvent being volatile. The evaporation of the solvent causes the viscosity of the remaining fluid to increase and

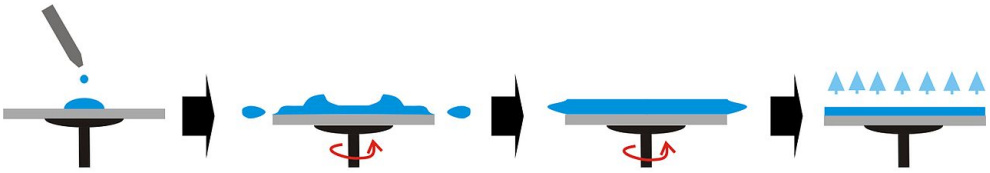

Figure 23: The process of applying thin film to a substrate using spin coating. Image from [14].

eventually it will be so high that the centrifugal force can no longer spread it any further out. The last step of heating to evaporate the remaining solvent can cause additional thinning but nothing substantial.

6.1.1 *Spin coating of PbS thin film*

For this project the coating material is the PbS NPs. As mentioned earlier they come in a toluene solution which acts as a solvent and is volatile so it will evaporate during the spin coating process. The PbS will not stick to the substrate by itself during spin coating, so a binding matrix is needed. A common and easy to use binding matrix is the polymer Poly(methyl methacrylate) (PMMA) also known as acrylic glass. The PMMA is mixed with the PbS in toluene solution, and dissolved therein, prior to be being spin coated. Once the toluene evaporates during and shortly after spin coating, the PMMA will solidify again and act as a host matrix for the PbS NPs.

Substrates used for samples are silicon and fused quartz. The silicon samples were cut from a double polished silicon wafer into roughly square pieces with a size of 1 cm^2. The quartz samples were about the same size. Prior to the substrates being spin coated, they went through a cleaning process to ensure a clean surface. This process involved putting the silicon and quartz pieces in a small beaker with a soapy DI water solution and using an ultrasonic cleaner for 5 minutes. This is repeated with acetone and isopropanol instead of the soapy DI water solution and finally the substrate is dried using N_2.

The specific samples made with spin coating will be presented in the next chapter, where their characteristics will also be discussed.

7

CHARACTERISATION OF PBS DEPOSITED ON SUBSTRATES

This chapter will deal with the characterisation of PbS NPs deposited on substrates. Structural characterisation through SEM imaging and profilometry, and optical characterisation through PL/PLE spectra and absorption measurements. This will lead up to the quantum efficiency measurements which will be presented in the next chapter. These measurements will in the end help us to decide whether or not the purchased PbS NPs will be suitable for use in a silicon solar cell using an erbium based upconverter.

7.1 INITIAL SAMPLES

Deposition of PbS in PMMA thin film

The first three samples were made with different amounts of PMMA added to the PbS in toluene solution. This was done with the intention to use SEM imaging to determine the coverage of PbS NPs on the silicon substrate. The first sample was made with a 1:1 ratio between PbS and PMMA, measured by their mass. The PMMA was in powder form and added directly to the PbS in toluene solution and given some time to allow for the toluene to dissolve the PMMA. A piece of silicon was cleaned using the process described in chapter 6.1.1 and placed in the spin coater. Using a pipette, the surface of the silicon substrate was covered with the solution and subsequently the spin coater was activated with a one minute program. The program started with 10 seconds at 1000 rpm to distribute the solution evenly across the surface, followed up by 50 seconds at 3500 rpm to remove the excess solution and create a uniform film on the surface of the substrate. Immediately after the spin coating, the sample was placed on a hot plate at 150 °C for one minute, to evaporate any left over toluene in the film. A second sample was made in the same way, but using a 1:3 PMMA to PbS ratio, and a third sample was made using no PMMA to see how it would bind to the surface without it. The third sample turned out as expected with no resulting thin film of the sample, only some spread out residue of the PbS solution, and it confirmed that a binding matrix is needed to spin coat a thin film of PbS NPs.

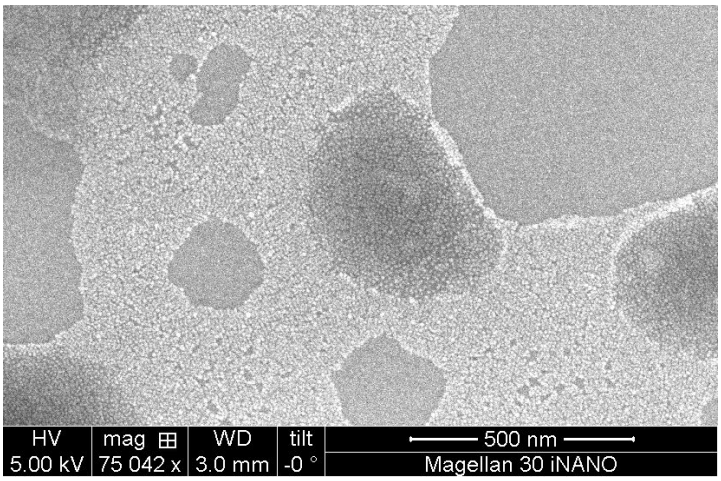

Figure 24: SEM image of 1:1 PMMA:PbS sample.

Structural characterisation

Next up is structural characterisation of the two samples with different PbS to PMMA ratios. SEM images was taken of both samples and can be seen in Figure 24 and 25. If we start by looking at Figure 24, it shows the sample with 1:1 PMMA to PbS ratio. It clearly shows the individual NPs on the silicon surface, but it is not completely covering the surface. The dark area in the middle of the image seems to have a lower density of NPs, while there also seems to exist areas completely devoid of NPs like in the upper right hand corner.

In Figure 25 is shown two images of the 1:3 PMMA to PbS ratio sample. Figure 25.a is a large scale view of the film and shows some odd looking dark areas of the film. A close-up image of a dark area is shown in Figure 25.b and it shows that the dark areas have a lower NP density compared to the lighter areas where it seems the NPs are lying as close as possible to each other. Based on this image, the diameter of the NPs were estimated to be roughly 7-7.5 nm with an average of 7.3 nm.

The dark areas of lower NP density appears in both samples and is believed to be caused by the heating of the samples that was done immediately after spin coating. The heating which took place at 150 °C would have caused the toluene to evaporate rapidly since toluene's boiling point is 110 °C, and this is believed to have caused the cracks in the film seen in the SEM images.

The thickness of the film on the two samples was then measured using the profilometer as described in chapter 4.3. In Figure 26 the profile measurement of the 1:1 sample can be seen with the scratch made in the film around 0.65 mm. The surface roughness makes it hard to determine a specific film thickness since it takes up a consid-

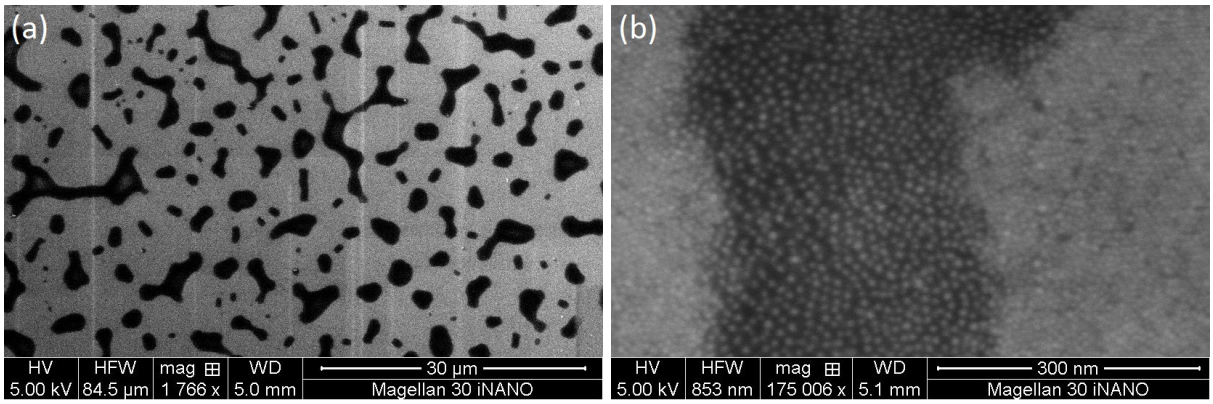

Figure 25: SEM images of 1:3 PMMA:PbS sample. The left image shows the general appearance of the film while the right one is zoomed in on one of the darker areas.

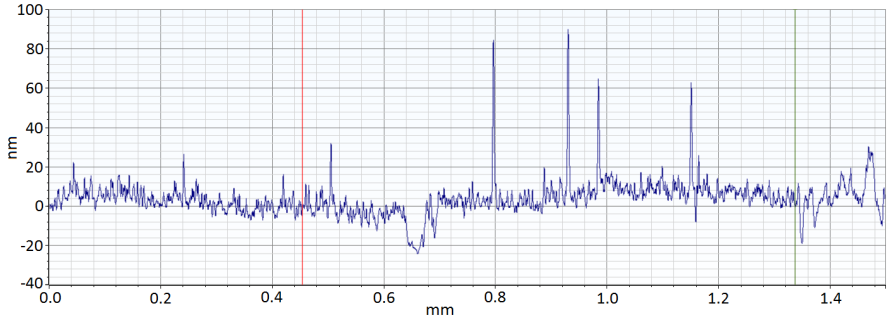

Figure 26: Profilometry measurement of silicon substrate with 1:1 PMMA to PbS ratio film spin coated on.

erable fraction of the total thickness. An approximation of the average film thickness to about 20-30 nm is the best that can done. This also agrees with the SEM images that does not show full coverage of NPs, if the PMMA to PbS ratio from the solution is assumed to be carried over in the film. This assumption would mean that about 13% of the volume in the film is PbS NPs based on their densities, 7.6 g/cm^3 for PbS and 1.18 g/cm^3 for PMMA. This implies the layer is not thick enough to contain a complete layer of PbS NPs since their diameter is about 7.3 nm.

The profilometry measurement of the 1:3 sample is shown in Figure 27. It shows a considerably higher surface roughness compared to the first sample, but also a thicker layer based on the two scratches made that can be seen in the profile just below 0.4 mm and 1.75 mm. The thickness is again a difficult parameter to determine with such high surface roughness, but is estimated to have an average thickness of 40-50 nm. In the same way as for the 1:1 sample, we can calculate the fraction of the volume occupied by the PbS NPs to about 32%. This increased fraction combined with the increased thickness means there is enough NPs to completely cover the surface of the silicon substrate.

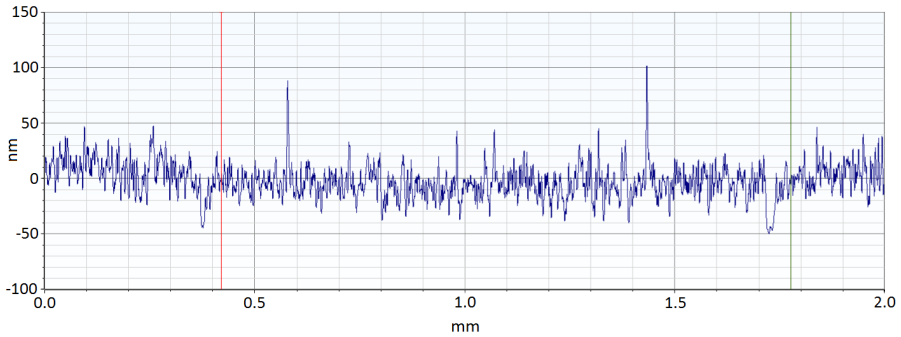

Figure 27: Profilometry measurement of silicon substrate with 1:3 PMMA to PbS ratio film spin coated on.

This is also seen from the SEM image shown in Figure 25.b where apart from the darker areas, the NPs are packed very close together.

The increased surface roughness of the 1:3 sample could be caused by the higher amount of NPs that would make it harder for the evaporated toluene to escape compared to the 1:1 sample where the NPs does not have full coverage. The toluene would push around the NPs when evaporating from inside the film, thus pushing some of it upwards near the dark areas in the SEM images. This is only speculation though and might not be the right explanation.

Optical characterisation

The optical characterisation of the NPs in a thin film is a very important part since it can tell us how the NPs have reacted to being deposited, if it has changed anything. As we saw above, the sample with 1:1 PMMA to PbS ratio did not have full NP coverage of the deposited film. The 1:3 ratio sample had much better coverage and was chosen to be used for optical characterisation.

The PL/PLE spectra that was supposed to be made with the monochromator set up was not possible to make though due to very little signal from the sample. The detector was not able to pick up any signal distinguishable from the noise. The PbS in PMMA film is too thin and the light power of the monochromator is not high enough to produce a measurable signal. Instead an 800 nm laser was used to illuminate the sample, with a much higher power. The higher power and an increasing of the detector slit width to 2 mm made it possible to get a good measurement.

An emission spectrum of the 1:3 ratio sample is shown in Figure 28. There appears to be two curves shown in this spectrum, it is however only one measurement and the cause for it is unknown. It is not caused by data analysis since the original measurement file has the same appearance and the effect will be ignored. The emission peak

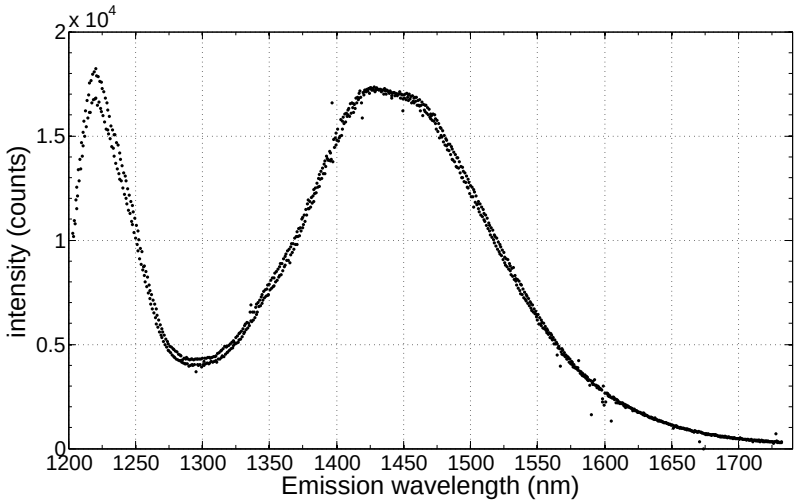

Figure 28: PL spectrum of 1:3 PMMA to PbS ratio film spin coated on silicon. Sample is illuminated using 800 nm laser with 140 mW power.

has moved to about 1440 nm, close to 100 nm shorter than the emission peak for the NPs while still in the toluene solution. There is also part of a second peak visible with its top point below the measured wavelength range. The peak is cut off by the 1200 nm long pass filter placed in front of the detector. This peak could be explained by de-excitation of electrons from the second excited state, which was also seen vaguely in the absorption spectrum of PbS in toluene in Figure 14. The reason it is not seen in the PL spectra shown in chapter 5.2 of PbS in toluene solution, is most likely due to the different source of excitation light. In the case of the PbS in toluene measurements the xenon lamp + monochromator was used compared to the 800 nm laser used here. The laser was used with a power of 140 mW while the monochromator set up delivers less than 6 mW at its highest value. The leftmost peak shrinks faster with reduced laser power and vanishes before the 1440 nm peak does. This agrees with the fact that we do not see it when using the monochromator set up as illumination source.

A series of spectra were taken with varying laser power to see how it affected the peak areas. The result is shown in Figure 29 on a double log scale. It is seen that the area of the leftmost peak, here named 1225 nm peak for its position, increases faster with laser intensity than the peak at 1440 nm. This tells us that the possible excitation to the second excited state in the conduction band, has a higher dependency on the laser power than the first excited state. The reason we do not see it using the monochromator set up, is simply because the power of

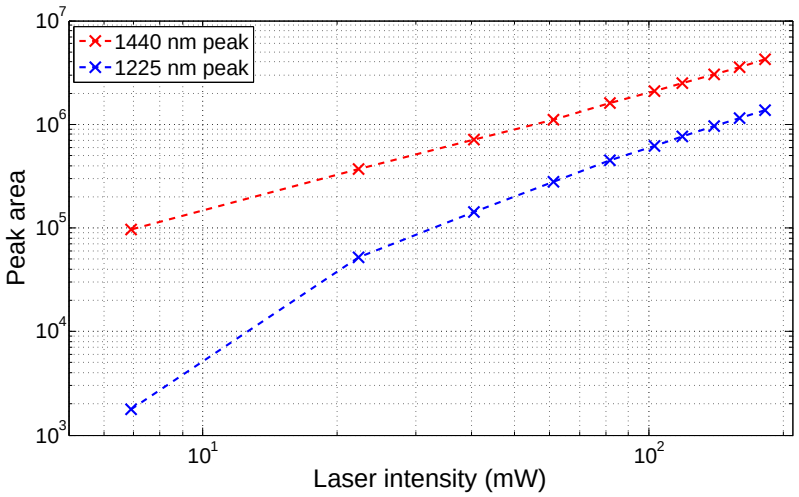

Figure 29: Areas of the two peaks present in Figure 28 as a function of laser power.

the excitation light is not high enough to excite enough electrons to produce a measurable signal when they de-excite to the ground state.

The fact that the emission peak got blueshifted most likely has to do with the change of the NP surroundings. In the thin film the NPs are packed closely together whereas in the toluene solution they were relatively far from each other. They are now also in a PMMA matrix instead of being suspended in toluene. The exact cause and mechanism of the blue shift is not completely understood, but is an obvious concern since the desired emission wavelength is 1500 nm to 1550 nm.

Since the laser had to be used, a PLE spectrum could not be made. The next step is to make samples with a higher signal that can be characterised using the monochromator set up as light source.

7.2 DROP CASTING OF PBS

The spin coating of PbS film on silicon discussed above yielded a too thin film as it was not possible to measure a PL spectrum using the monochromator set up for broad band illumination. Two new samples were made without spin coating, but instead just drop casting PbS onto silicon substrates. The first sample used the same 1:3 PMMA to PbS ratio solution as mentioned above, while the second sample was made without PMMA. The second sample without PMMA was also made with the intention to show the effect of PMMA on the prop-

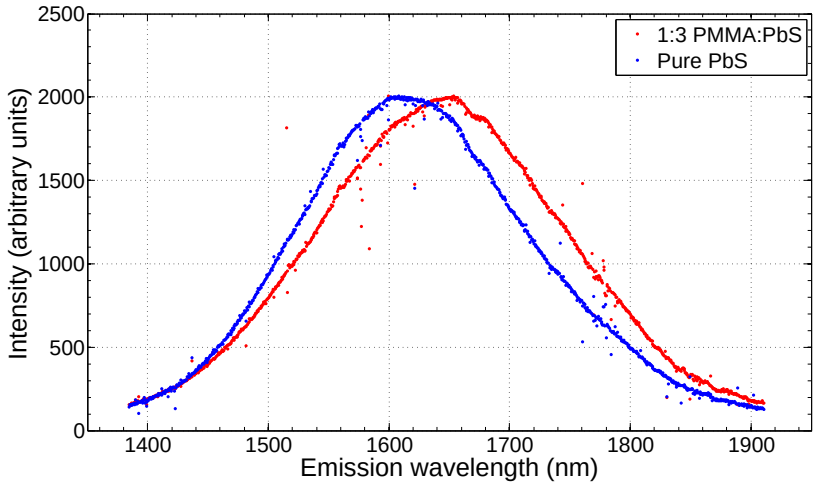

Figure 30: Emission spectrum of the two drop casted samples taken at 1000 nm excitation wavelength. They have been scaled to match each other.

erties on PbS, and since drop casting was used the PMMA was not necessary for the PbS to stick to the silicon surface.

The samples were made by placing the silicon substrate on a hot plate at 90 °C and then dropping the solution onto the substrate using a pipette. The toluene appeared to evaporate fairly quickly, it took no more than a second before the liquid had seemingly dried on the substrate. The result was a very uneven layer of NPs due to the "coffee ring effect" of several drops overlapping with each other. Even after a minute on the hot plate and several days at room temperature, the PbS layer had not hardened on the silicon surface. It was not possible to make a scratch in the layer without it rubbing off on the scalpel, and if measured with the profilometer it would have contaminated the stylus tip since it was sticking to anything in contact with it. The thickness however must have been several tens of μm in some places since the surface topography was clearly visible to the naked eye.

This did not prevent PL measurements, and the layer was also thick enough to make broad spectrum measurements using the monochromator set up. This allows us to see the effect of the PMMA on the optical properties of the NPs. The emission spectrum of the two samples is shown together in Figure 30. The emission wavelength is slightly redshifted for the sample containing PMMA compared to the sample without PMMA. The PMMA surrounding the PbS NPs seem to affect the energy levels, lowering them.

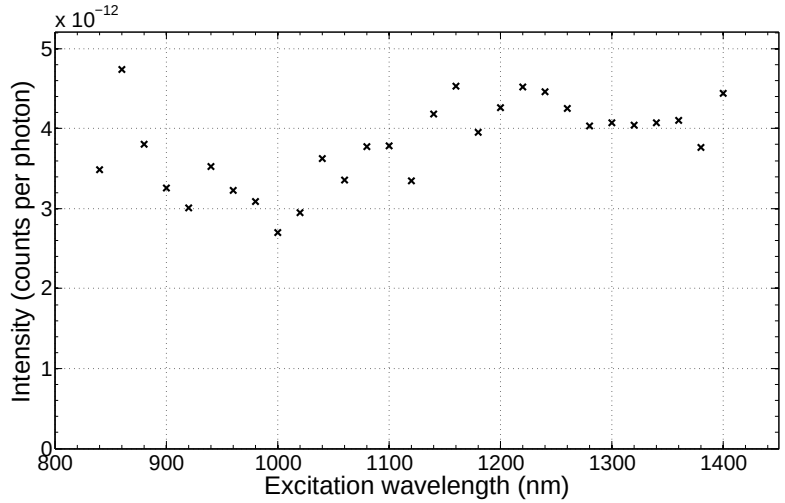

Figure 31: PLE spectrum at 1640 nm of drop casted sample with 1:3 PMMA:PbS ratio.

PLE spectra were also made both for the sample with PMMA and the one without, and they are shown in Figure 31 and 32 respectively. They look very much like each other, and are relatively flat, with a slight increase towards higher wavelengths for the sample with PMMA. Since the PbS layer on both samples were fairly thick, they seem to absorb most of the light. The penetration depth for the two different PbS concentrations at 1200 nm can be calculated using the cross section found in chapter 5.1.1 and are roughly 6 µm for the sample containing PMMA and 2 µm for the sample without PMMA. This is less than the estimated thickness of the samples and thus also points towards all of the light being absorbed.

These two samples made with drop casting have a much higher emission wavelength than the spin coated sample discussed in the previous section. A 200 nm difference in emission wavelength between the spin coated 1:3 ratio sample and the drop casted one. The structural difference between the two being the thickness of the film, and possibly the surroundings of the NPs. In the spin coated sample, the SEM images showed the NPs being packed very closely together, possibly in a single layer due to a very thin film. In the drop casted sample the film was very uneven and much thicker than the spin coated one, most likely the NPs would not be arranged in neatly packed layers. This makes their surroundings different based on different deposition methods. Another difference between them is the heating temperature applied to evaporate the toluene from the sub-

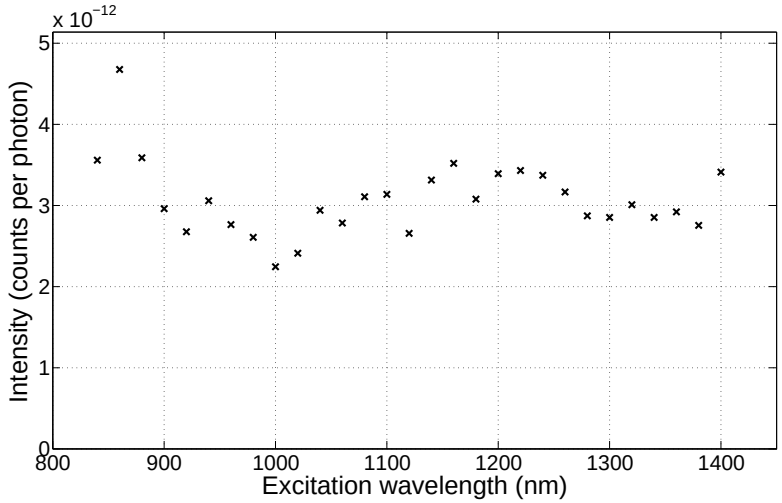

Figure 32: PLE spectrum at 1600 nm of drop casted sample with only PbS.

strate. Exactly how each of these affect the NPs is unsure but their overall effect seems to be a change in the emission wavelength.

The next step is to make spin coated samples with a much higher thickness. For the NPs to be used as a downshifting layer in a solar cell, they need to absorb all the light coming through the layer for maximum efficiency. The spin coated samples with 50 nm or less thickness is not nearly enough for this and thus thicker samples will need to be made with spin coating.

7.3 VARIATION OF SPIN COATING SPEED

For the NPs to be used as a downshifting layer in a solar cell, the layer needs to absorb as much light as possible. The thickness needed for absorbing 95 % of incoming light is three times the penetration depth. For pure PbS NPs this is about 6 µm based on the cross section for the NPs in toluene solution. This is the thickness without PMMA added in to allow it to be spin coated on to a substrate, which means an actual spin coated PbS in PMMA film will have to be much thicker. To measure the quantum efficiency of the NPs we might not need to absorb 95 % of the incoming light, but the layer definitely needs to be thicker than the initial spin coated samples.

There are various ways to increase the thickness of the spin coated film, with the most obvious one being decreasing the spinning speed. Another factor is the viscosity of the liquid, which reduces the centrifugal force's ability to push the fluid off the sample. The viscosity

of the toluene solution containing the PbS NPs can be slightly increased by evaporating some of the toluene, thus increasing the NP concentration. The increased concentration also increases the amount of NPs that will be dropped onto the sample prior to spinning it.

Some PbS in toluene solution was heated to evaporate some of the toluene and ended with a new concentration of 24 mg/mL, 2.4 times higher than the original concentration. PMMA was added in a 10:1 PMMA to PbS ratio to increase the amount of PbS NPs that could be bound to the substrate. Four samples were to be made, with different maximum spin speeds to see the connection between spin speed and film structure. The samples were made by the same method described in section 7.1, except the second stage of spinning for 50 seconds would be done at different speeds. The four samples, which shall be named A, B, C, and D were made at maximum speeds of 1500 rpm, 2000 rpm, 3000 rpm, and 4000 rpm respectively. The first 10 seconds of spinning was at 1000 rpm for all four samples, and the subsequent heating on the hot plate was done it 50 °C.

Sample A had a ring around the edge of the silicon substrate of extra thick PbS in PMMA layer. The 1500 rpm maximum spinning speed was seemingly not enough to overcome the surface tension at the edge. The film in the middle of the substrate seemed grainy. Sample B did not have the complete ring, but only at the corners were there excess solution. Sample C and D both had nearly no excess solution at the corners, and the film seemed much smoother than first two.

Similar samples were attempted to be made on quartz, but the NPs and PMMA did not stick to the quartz surface as well as on the silicon during spin coating. The absorption measurements of the quartz samples showed little to no absorption for all wavelengths and the rest of the characterisation of spin coated samples will only deal with silicon samples.

Profilometry measurements of the film are shown in Figure 33 for all four samples. There is a clear difference in the surface roughness of the four samples. Sample A has very high roughness and determining the thickness is very tricky. The depth of the scratches made seems to be just under 2 µm based on the chosen zero-line. This is just a measure of the minimum thickness though, and the average thickness is higher than that. If we look at the other samples, the surface roughness decreases as the maximum spin speed is increased, and for sample D the surface is relatively smooth with roughness much smaller in scale compared to the film thickness. The minimum thickness of the layers seems to actually increase as the spinning speed is increased, contrary to what was stated earlier. Sample D has a very smooth surface with the only irregularities coming from the coating material pushed aside when making the scratch, and thus the shown thickness in profilometry measurement is the actual thickness. For the

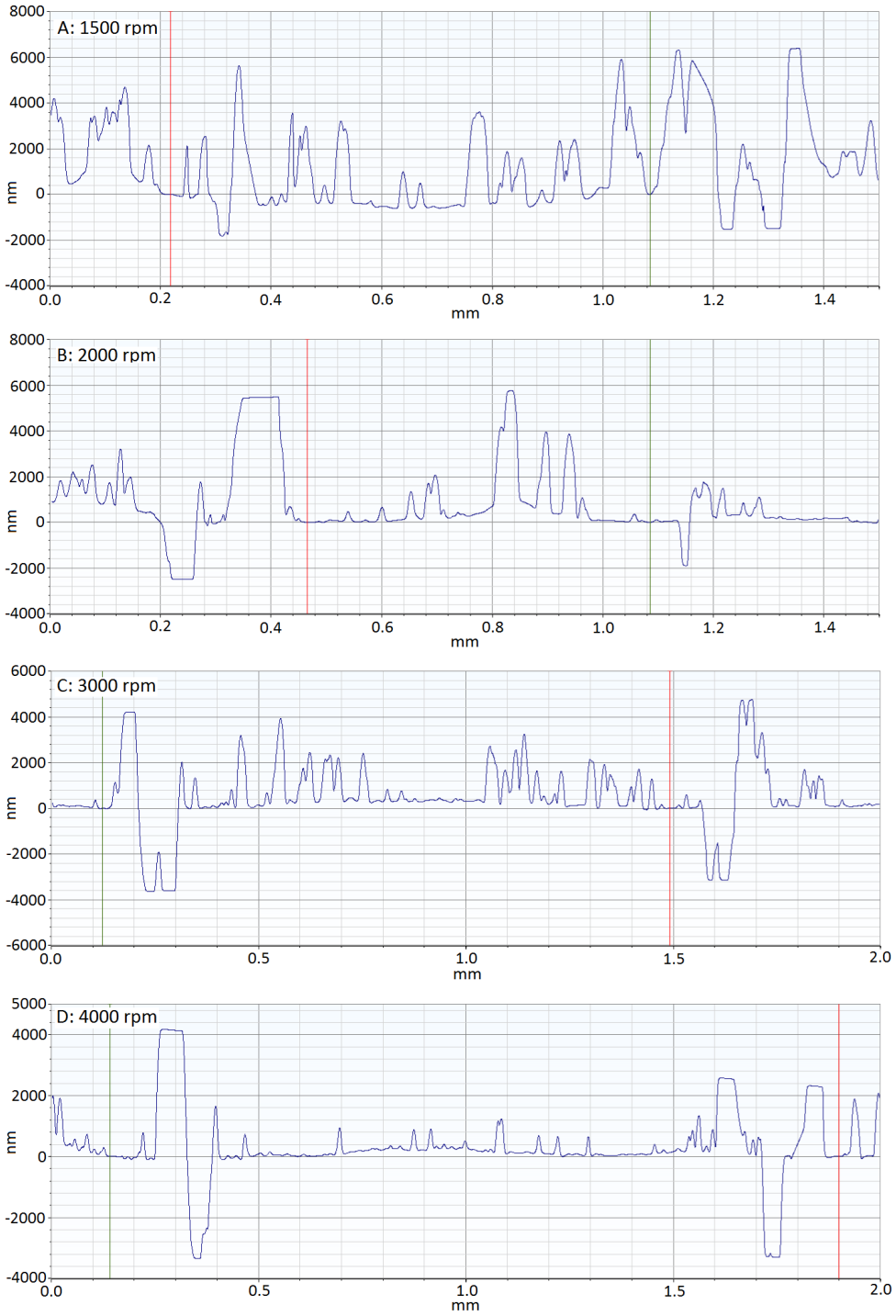

Figure 33: Profilometry measurements of samples A, B, C, and D, made with a maximum spin speed of 1500 rpm, 2000 rpm, 3000 rpm, and 4000 rpm respectively.

other samples the actual thickness is harder to determine because of the increased roughness. The effect of the increased spin speed then seems to have been to create a more even distribution of the PbS in PMMA coating on the substrate surface. This could mean that the 10 seconds of spinning at 1000 rpm at the beginning of the cycle had a high impact on the thickness of the samples, and that the high spin portion of the cycle did not push any substantial amount of the solution off the substrate, but instead smoothed the surface out. This is probably caused by the evaporation of toluene prior to spin coating, which increased the concentration of both PbS and PMMA which in turn increased the viscosity of the solution. The first 10 seconds at 1000 rpm was then enough time for further toluene evaporation to the point of increasing the viscosity enough for the centrifugal force to not be able to push more solution off the substrate.

7.3.1 *Absorption measurements*

Absorption and emission measurements were also made for the four samples. The transmittance and reflection of sample C is shown in Figure 34, along with the absorption calculated by subtracting the reflection and and transmission from the 100 % transmission baseline. The silicon substrate dominates the absorption at and below the silicon band gap, while it absorbs practically nothing from 1200 nm and above. The absorption has the expected peak at 1500 nm but also seems to have smaller peaks around the 1500 nm one. The smaller peaks comes from the variation in reflection which is most likely caused by thin film interference. This is interference between light reflected at the surface of the coating and light reflected at the surface of the substrate. The difference in path length determines whether there is constructive or destructive interference. If the path length difference is an integer multiple of the wavelength, there is constructive interference while if it is a half integer multiple, the two waves will be 180 ° out of phase and cause destructive interference.

This only shows up in measurements if the film has a uniform thickness, since it otherwise would average out and cause neither constructive nor destructive interference. The same effect is seen in sample D while for sample B there is only the small ripples seen from 500 nm to 900 nm. Sample A does not show any interference effects at all. This confirms the conclusions of the profilometry data discussed above, that the increased spin speed significantly reduced surface roughness. Sample A and B have enough roughness so that the film does not have an even enough thickness for measurable interference effects to occur, partly because the light gets scattered due to the uneven surface and thus the path length of the light varies a lot. Sample C and D have a much smoother surface which means the

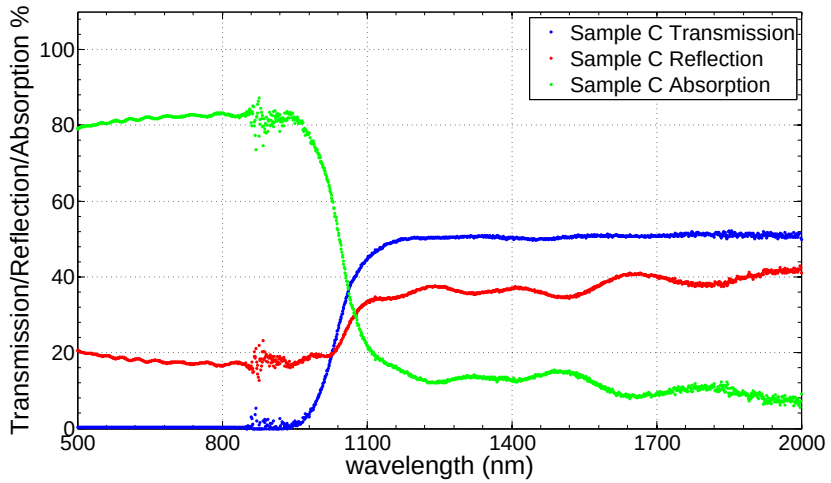

Figure 34: Transmission and reflection measurement of sample C. Absorption is calculated by subtracting the transmission and reflection from the baseline (100 % transmission).

thickness is almost the same everywhere, and this means the path length for light going through the film is nearly the same for all photons.

Calculation of the absorption coefficient is not so straightforward since it requires a specific thickness of the coating. The uneven surface of the spin coated samples makes it hard to assign a thickness to the coating. A drop casted sample was made on quartz in an attempt to get a sample with a known thickness. It was made with the same 10:1 PMMA to PbS ratio that was used for samples A, B, C, and D. A drop of the solution was applied to a piece of quartz and spread out to cover the whole surface. Then it was allowed to dry without heating it, to avoid the uneven surface of the previous drop casted samples. This created a very smooth and glossy surface, and profilometry measurements showed a thickness of 13 µm.

In Figure 35 is shown the calculated absorption coefficients of the four spin coated samples of varying spin speed, along with the drop casted quartz sample named sample X. The thickness of the spin coated samples were estimated from the profilometry measurements. Sample C and D had very little surface roughness, and the used thickness is 3.2 µm for sample D and 3.5 µm for sample C. For sample A and B and estimate of 3 µm was made for both samples based on the minimum thickness and the surface roughness.

The calculated absorption coefficient of sample D and sample X seem to match fairly well, except for the ripples on the curve for sam-

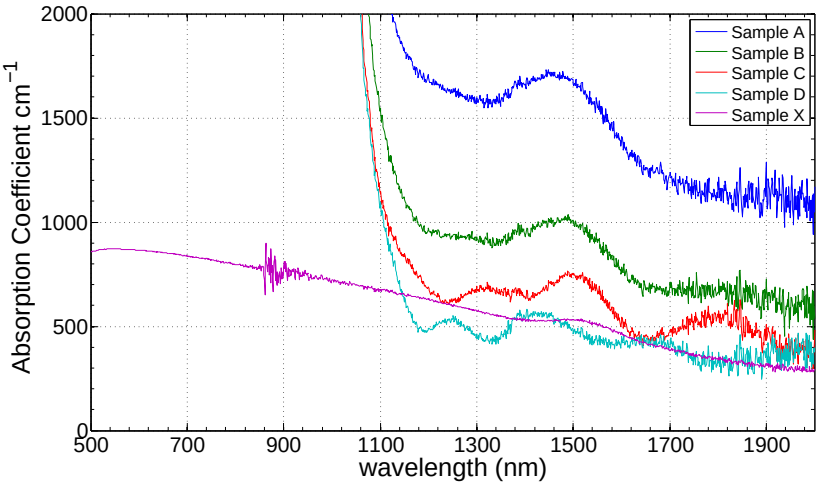

Figure 35: Absorption coefficients of the four samples made with varying spinning speed.

ple D which is not fully understood, but could come from interference effects. The absorption coefficient for these two samples is believed to be the correct value, while the higher absorption measured in sample A, B, and C is believed to be caused by the increased path length of the light through the film. The increased surface roughness scatters the light more, and causes the light go through the film at an angle which increases the path length and allows for more absorption.

The cross section can also be calculated and for that we need the particle concentration. The PMMA to PbS ratio was 1:10 in the toluene solution so if we take an example with 1 mg PbS and 10 mg PMMA we can calculate the total volume using their densities, 7.6 $\frac{g}{cm^3}$ for PbS and 1.18 $\frac{g}{cm^3}$ for PMMA.

$$\frac{1\ mg}{7.6\ \frac{g}{cm^3}} + \frac{10\ mg}{1.18\ \frac{g}{cm^3}} = 8.6 \cdot 10^{-3}\ cm^3$$

The amount of NPs in 1 mg of PbS is calculated from their average diameter of 7.3 nm and gives a particle concentration in the film of

$$7.5 \cdot 10^{16}\ \frac{particles}{cm^3}$$

Using this and an absorption coefficient of 530 cm^{-1} at 1500 nm, we get the cross section at 1500 nm to be $7.1 \cdot 10^{-15}$ cm^2. This is about 6.5 times higher than the measured cross section for PbS in the toluene solution which was $1.1 \cdot 10^{-15}$ cm^2. The deposition of the NPs in the PMMA film has seemingly increased their absorption

and it is not understood exactly what is the cause of this. The absorption coefficient curve is also more flat than for PbS in toluene, which showed almost practically zero absorption above 1700 nm. It could be an increased scattering of the light for the transmission measurement, where light that is scattered and exits at an angle close to parallel to the sample would not be caught by the integrating sphere that collects the light. The sample was placed right at the edge of the sphere, in an attempt to try and eliminate this loss as much as possible. This loss of scattered light would not be only above 1700 nm though, but across all wavelengths which mean it could also have contributed to the increased absorption cross section measured, compared to the NPs in the toluene solution.

7.3.2 *Photoluminescence measurements*

PL spectra were made with the monochromator set up for all four spin coated samples and they are shown together in Figure 36 where they have been scaled. The small peak present on three of the curves at 1760 nm is believed to come from the lab set up in some way since it is not present on all samples, and vanished for excitation wavelengths above 1200 nm. The four samples have close to the same emission wavelength, varying between 1590 nm and 1620 nm. This is red shifted about 50 nm compared to emission from the NPs while still in the toluene solution, even though the absorption coefficient peak is located just below 1500 nm for both cases.

In Figure 37 is shown the PLE spectrum measured for sample C, normalised to the incoming amount of photons. This is nothing like the previous PLE spectra seen, this is showing a rather large increase in emission intensity for increased excitation wavelengths. From 1000 nm to 1200 nm it almost doubles in emission intensity while the absorption showed no such jump in that range, assuming it follows the same general trend as sample X. One thing that has not been tested yet, is the validity of the normalisation used. The measured counts from the detector has been normalised to power of the excitation light, which is more than an order of magnitude higher for shorter wavelengths as was seen back in Figure 6. The power curve of the monochromator set up also has small peaks at 1180 nm and 1260 nm where the power is twice as high compared to 20 nm above or below these peaks. This is seen in most of the PLE spectra where the corresponding normalised emission intensity for excitation wavelengths of 1180 nm and 1260 nm is lower than the data points next to them. This would indicate that the emission intensity is not proportional to the power of the excitation light.

To test this, a series of measurements were done on sample C with varying power of the excitation light, to see if 10 times higher excitation light power, corresponds to 10 times higher peak area. It was

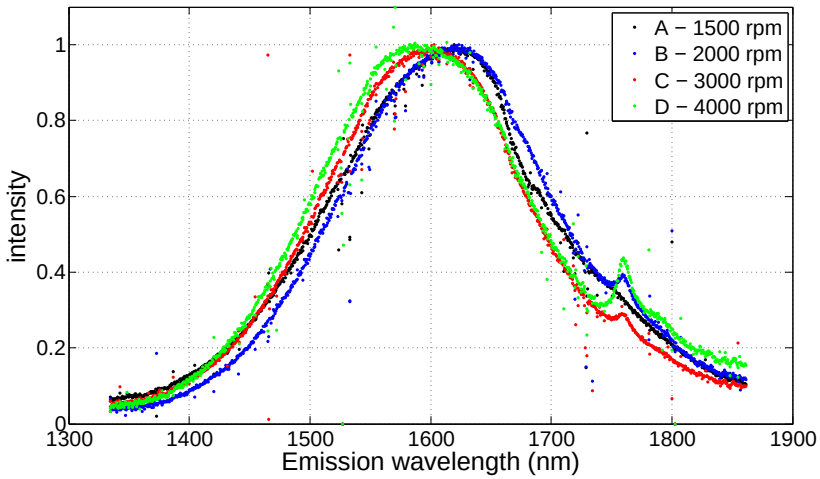

Figure 36: Emission spectra of samples A, B, C, and D taken at 1100 nm excitation wavelength. The small peak at 1760 present on some of the samples are believed to come from the lab set up, and not from the samples themselves.

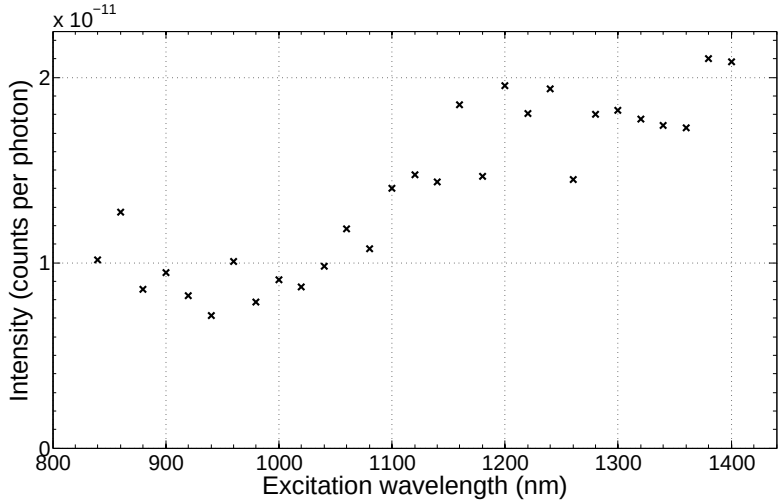

Figure 37: PLE spectrum of sample C taken at 1600 nm emission wavelength.

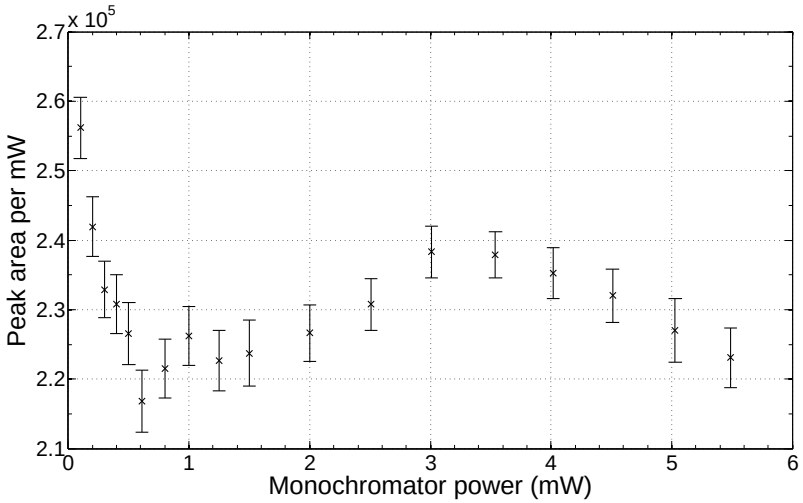

Figure 38: Peak area measured as a function of power of the excitation light. Measurement done on Sample C at 900 nm excitation light.

done at 900 nm excitation wavelength since the power at 900 nm was high enough that by using an attenuation filter the power could be varied more than an order of magnitude while still getting enough signal from the sample. A rotating attenuation filter was placed in the beam path just before the sample to control the light power. The filter had a smooth attenuation gradient when rotated, but unfortunately there was a few cracks in the filter which seems to have affected the outcome. The peak area was was measured 10 times for each power value and then an average was calculated along with the standard deviation. The result is shown in Figure 38.

While the peak area per mW only varies by around 10 % over most of the power range, the variation looks like a systematic variation and not a random one. This is believed to be caused by the cracks in the attenuation filter, which when placed in the beam path caused the beam to be scattered, resulting in a different spatial distribution of the beam power across the sample surface. Even with this variation believed to be caused by the cracks, the overall variation in peak area per mW is so small that it can not be the cause of the variation in the PLE spectrum seen in Figure 37.

The lower emission intensity at 1600 nm for shorter excitation wavelengths could maybe be caused by absorption in the second excited state, and then a direct transition to the valence band emitting a photon of shorter wavelength than 1600 nm. This would reduce the emission at 1600 nm for excitation wavelengths above the energy of the second excited state. However no emission peak was observed beside

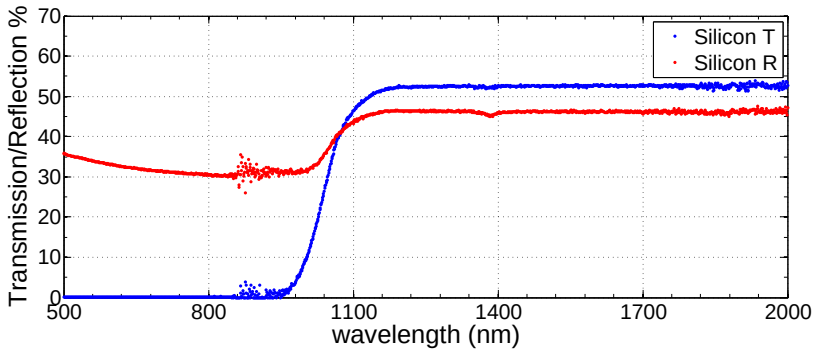

Figure 39: Transmission and reflection of polished silicon wafer with a thickness of 300 µm

the one at 1600 nm, most likely due to the quick relaxation process responsible for lowering the energy of the electrons to the bottom of the conduction before they make a transition to the valence band.

The film is deposited on silicon which reflects a relatively high amount of the incident light. A transmission and reflection measurement made on a bare piece of silicon like the ones the samples were made on, are shown in Figure 39. This shows an increase in reflection from 31 % to 46 % in the wavelength range from 1000 nm to 1150 nm. This range nearly matches with the range in which the PLE spectrum in Figure 37 is increasing. So photons that go through the PbS in PMMA film without getting absorbed can be reflected and travel through the film again, giving it another chance to be absorbed. The increased reflectivity above 1000 nm will then result in increased absorption that could be part of the reason higher emission intensity is measured for higher wavelengths.

The result of these samples with PbS deposited on substrates shows that the deposition definitely has an effect on the optical properties of the NPs. The initial spin coated film with a 1:3 PMMA to PbS ration was very thin and had NPs packed closely together, and showed a blue shift of the emission wavelength. The other samples were made with much thicker films that contained higher amounts of PMMA per NP and these samples showed a little red shift of the emission wavelength compared to in the toluene solution. The drop casted samples supported the fact that PMMA increases the emission wavelength. Varying the spin coating speed showed a big difference in the surface

roughness of the film, with increasing roughness increasing the surface scattering.

The big question though, that will ultimately decide whether the NPs are suitable for use in a downshifting layer, is their quantum efficiency (QE). If their QE is too low, they will not provide enough increased efficiency for the entire solar cell to be worth implementing. The next chapter will be describing the process of making the QE measurements and discuss the results.

8

QUANTUM EFFICIENCY

The big question, and probably the most important aspect of the NPs is their QE. This chapter will describe the process of measuring the QE and the goal is to be able to give an estimate of the NPs QE to within an order of magnitude. This will help decide whether they are suitable for use in a downshifting layer or not.

Measuring the QE is done with the integrating sphere which is described in chapter 4.1. The sample is placed within the sphere and an 800 nm laser is used as excitation light. Placing the sample within the sphere reduces the measured emission light, and the monochromator set up does not provide enough excitation light power to produce a measurable emission signal, so the laser had to be used. Ideally the excitation wavelength should have been in the 1100 nm to 1500 nm range, since that is where the NPs are needed to downshift the sunlight. Measurements were done on the four samples A, B, C, and D.

Besides measuring the emission from the samples placed in the sphere, an energy calibration has to be made. The energy calibration will allow us to translate the peak area measured by the detector, in to how much energy was emitted by the sample. This is then compared to the amount of energy hitting the sample to create the measured peak area, to get the QE. The energy calibration was done with a 1500 nm laser which is as close to the emission wavelength of the samples we can get. The laser is pointed in to the sphere with no sample inside. The laser light is then scattered randomly inside the sphere and the detector measures how much is coming out of the sphere. This serves the purpose of simulating the light emitted by the samples, namely a specific amount of light, the laser power. The measured peak area can then be divided by the measured laser power and we get a calibration of how much energy is emitted from a sample that creates a specific peak area.

The signal from the samples in the sphere was very weak even though the power of the 800 nm laser was around 570 mW, an example is shown in Figure 40 for sample D. In the figure is also shown the result of applying a median filter to the data. This was done to remove large spikes coming from background noise. While the data points shown already have been corrected with a background spectrum, there was still spikes from background noise that varied from each measurement. 10 spectra were taken with each sample and the average peak area was calculated from the filtered data.

Along with the energy calibration made with a 1500 nm laser, this allows us to calculate the power of the light emitted from the samples.

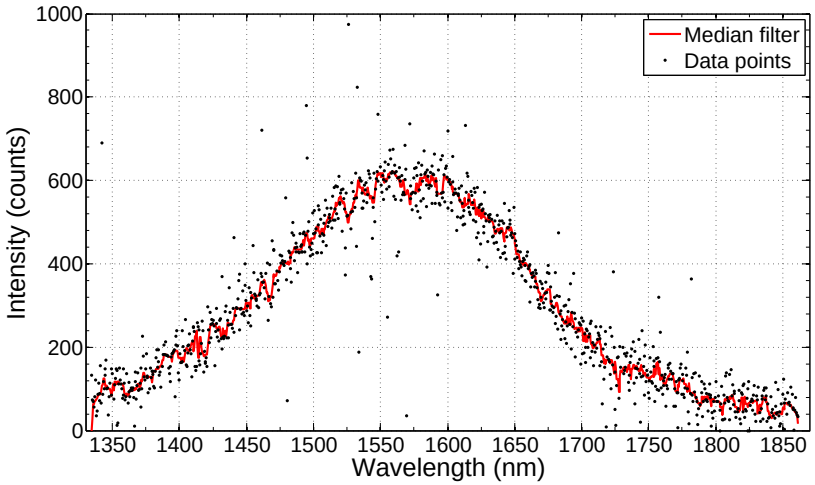

Figure 40: Emission spectrum of sample D while in the integrating sphere. Also shown is the result of applying a median filter to the data, to filter out the large spikes caused by background noise.

Sample	EQE
A	$(1.5 \pm 0.12) \cdot 10^{-4}$
B	$(8.4 \pm 0.76) \cdot 10^{-5}$
C	$(7.9 \pm 0.72) \cdot 10^{-5}$
D	$(8.0 \pm 0.74) \cdot 10^{-5}$

Table 1: External quantum efficiencies for the four samples made with varying spin speed.

This then makes us able to get the external quantum efficiency (EQE) of the samples as the ratio between the outgoing amount of photons and the incoming amount of photons. The results are shown in Table 1 for all four samples.

The samples all have very low EQE, with sample A having almost twice as high efficiency as the others. Sample A being better than the others were expected from the absorption measurements that showed it to absorb more light then the rest. This was most likely due to the high surface roughness that increased the path length through the film, and is also believed to be the reason for the higher quantum efficiency.

The low EQE of the samples does not necessarily mean the PbS NPs can not be used. It could just be that samples need to be thicker or

Sample	a (cm^{-1})	absorption % at 800 nm	IQE
A	2100	47	$3.3 \cdot 10^{-4}$
B	1200	30	$2.8 \cdot 10^{-4}$
C	900	27	$2.9 \cdot 10^{-4}$
D	700	20	$4.0 \cdot 10^{-4}$

Table 2: IQE of the NPs in each of the four spin coated samples. The absorption coefficient (a) shown is for 800 nm and is estimated from the data available for higher wavelengths.

contain a higher PbS concentration in the film. To determine the QE of the particles themselves and not just the samples, the amount of photons actually absorbed in the sample needs to be determined. The ratio between the absorbed photons and emitted photons is the internal quantum efficiency (IQE) and is the one we are most interested in.

Since the film is deposited on silicon we do not have the absorption coefficient at 800 nm, but using the data we have for absorption we can extrapolate to lower wavelength. This is deemed reasonable since both absorption of PbS in toluene and PbS in PMMA drop casted on quartz (sample X) increases almost linearly from 1200 nm to 800 nm.

The value of the absorption coefficient for each sample at 800 nm is estimated from their values and slopes in the range where they are available. From that the absorption % in each sample can be calculated using

$$1 - A = \cdot e^{-L*a}$$

with L being the thickness of the samples used to calculate their absorption coefficient. In Table 2 the estimated absorption coefficient (a) are shown together with the calculated absorption % and the IQE found by dividing the previously shown EQEs with the fraction of light being absorbed.

Calculating the IQE did not make much of a difference since the samples absorbs a relatively large fraction of the light. They did however get closer to each other, which is expected since the only difference is the thickness of the film and surface roughness, both of which are not expected to affect the efficiency of the NPs. The slight differences still present is most likely caused by the estimate of their thickness from the profilometry data, and the extrapolated absorption coefficients. A thing that has not been taken into account is the reflection of light at the interface between silicon and the PbS in PMMA film, which causes increased absorption and would cause a reduction in the IQE. As a result the IQEs are a rough estimate, but is believed to be accurate within an order of magnitude.

When using 800 nm excitation light, there could also be the possibility of electrons making a transition from higher excited states to the valence band, possibly emitting a photon with a higher energy. Measurements however did not show any emission of higher energy photons. The relaxation processes that causes the electron to lose energy by lattice interactions do happen on a much shorter time scale (10^{-12} s) than the fluorescence life times (10^{-9} s), which could explain why it is not observed here. As was seen in chapter 7.1 a sample made with spin coating of a 1:3 PMMA to PbS solution did show emission of photons at a shorter wavelengths, which was assumed to come from the second excited state. That sample does have quite different properties than samples A, B, C, and D in general though, with a much thinner film containing a higher concentration of NPs.

A thing that has not been discussed yet is the spectral response of the optical equipment used to collect the light emitted from the samples. This is relevant since the energy calibration and the emitted light is not all at the same wavelength. The mirrors used to direct the light to the detector and also used inside the detector are silver mirrors, and their reflectance vary by 1-2 % at most in the 1400 nm to 1700 nm range. The diffraction grating used in the detector has a bit higher variation, it has an efficiency ranging from 70 % to 85 % in the same range. This will have caused a little change in the shape of the peaks but no relevant change in the calculated QEs. The detector itself has a variation of about 5 % in its QE over the mentioned range, so also small enough to not cause a significant difference in the outcome.

It can be conclude from these measurements that the NPs have a very low QE when placed in a PMMA matrix, too low for being usable in a solar cell for downconversion. A relevant question is then, what is the QE of the NPs in the toluene solution. It could just be that the handling of the NPs and the method of deposition has caused them to degrade and lower their QE. The QE of the NPs in toluene solution could be measured using the sphere as well, however this is very risky since it is a liquid and if spilled inside the sphere it is ruined. The best that can be done here is an attempt to compare PL measurements that has been performed on both the PbS in toluene solution and the deposited NPs.

The measured PL spectra for the two cases should be comparable since they have the same integration time, slit width, and illumination power. The challenge is to estimate the amount of light absorbed in the two cases, and how much of the emitted light is being picked up by the detector. In Figure 41 is shown the two measured emission spectra at 1100 nm excitation, and their areas are $3.8 \cdot 10^5$ and $1.9 \cdot 10^6$ for PbS in toluene and sample C respectively.

This shows a higher measured signal from the spin coated sample, which only absorbs about 24 % of incident light if we estimate an absorption coefficient of 800 cm^{-1} at 1100 nm. The cuvette containing

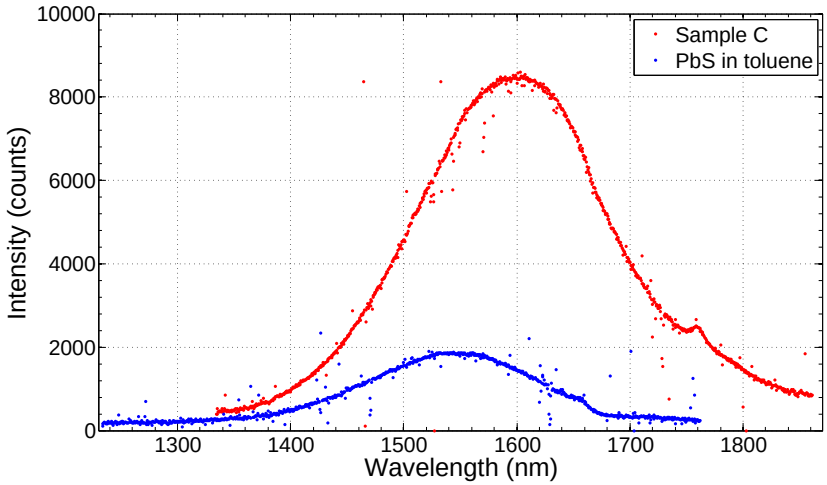

Figure 41: PL spectrum of sample C and PbS in toluene in a cuvette.

the PbS in toluene solution will reflect some of the incident light, but only about 5 % since the incident angle is close to 40 °. For light entering the cuvette it is fair to assume total absorption since the path length of the cuvette is 10 mm and the penetration depth at 1100 nm in the PbS in toluene solution is roughly 1.2 mm for absorption in PbS alone. While almost all the light gets absorbed in the cuvette, it is not all of it that will exit it again. The angle for total internal reflection when going from the quartz to the air is 41 ° which means light emitted from some NPs can not possibly reach the detector due to total reflection inside the cuvette. The answer to how much of the light emitted by the NPs reaches the detector compared to sample C is not so easy to find.

Instead we can assume they have the same QE, and then calculate how much of the light should escape the cuvette to create the measured peak area. Sample C absorbs 24 % of the incident light, which at 1100 nm is 0.24 mW, and we can multiply that by the IQE found above, assuming it does not vary too much when increasing the excitation wavelength, to get the power of the emitted light to $7 \cdot 10^{-8}$ W. This emitted power combined with a 1.5 s integration time generates the peak shown for sample C in Figure 41, which has an area of $1.9 \cdot 10^{6}$. The sample holder is placed approximately 5 cm from the collection lens which has a radius of 2 cm. It will be assumed that the emitted power is spread evenly in all directions from sample C, which means 4 % of the emitted light will be collected. If we do the same for the cuvette measurement, where we assume 95 % absorption and the same IQE, the emitted power is found to be $2.7 \cdot 10^{-7}$ W. The

peak area of the cuvette measurement is $3.8 \cdot 10^5$. This shows that the NPs in the toluene solution will emit about 4 times more light than sample C, while it only generates a peak area that is 20 % of sample C's peak. To get the measured peak for PbS in toluene, 0.2 % of the emitted light should be collected by the lens. If this value of 0.2 % seems too high, then the QE of the PbS NPs in toluene was higher prior to being deposited.

The above should be taken with a grain of salt, it is not claiming a specific QE of the NPs in the toluene solution, but merely a quick back of the envelope calculation to gain an estimate of their efficiency before they were deposited in the PMMA film.

The reason for the low QE of the NPs most likely lies with the passivation. They are passivated using oleic acid, which is organic ligands that bind to the surface atoms of the NP, in order to remove dangling bonds that introduce trap states in the band gap. This was also mentioned in chapter 3.2. The problem with the organic ligands is their thermal instability and photodegradation, which break up the bonds between the oleic acid and the surface of the NP, resulting in surface defects that introduce trap states. Results have been shown where the oleic acid ligands are replaced by halide anions, resulting in reduced density of trap states within the band gap, and thus an increased QE [15, 23].

To reduce the degradation of the organic ligands, maybe the heating step after spin coating could be omitted, and instead let the film dry at room temperature. Otherwise the solution could be to use different NPs, the core/shell type NPs show higher chemical robustness and are less susceptible to passivation degradation [17]. This is due to the outer shell of higher band gap material that efficiently passivates the surface states, and it also reduces the effects of the surroundings on the NP. Core/shell NPs have shown very high QE near unity [4, 8].

9 CONCLUSION

Majority of the solar cells manufactured today are silicon based. This gives them an inherent inability to convert the part of the sunlight with wavelengths above the silicon band gap at 1100 nm. Part of the solar spectrum above 1100 nm can be utilised using erbium based upconverters, but it is only a small fraction of it. By introducing a fluorescent layer containing downshifting NPs, the range between the silicon band gap and erbium absorption can be shifted into the absorption range of the upconverter. Commercially available PbS NPs are a possible candidate to use in the fluorescent layer and this project revolved around their characterisation.

Characterisation was done on the NPs still suspended in the toluene solution. Absorption spectra showed a first exciton absorption peak at 1500 nm and an increased absorption towards shorter wavelengths. The absorption cross section at 1500 nm was found to be $1.1 \cdot 10^{-15}$ cm^2. PL measurements showed that the NPs had an emission wavelength centered around 1550 nm with a FWHF of 180 nm, even though they were advertised to have an emission wavelength of 1600 nm. Emission at 1550 nm is close to optimal though since erbium upconverters mainly absorb from 1500 nm to 1550 nm.

NPs were then deposited in a PMMA matrix on silicon substrates using spin coating. Initial samples with 1:3 PMMA to PbS ratio created a thin film with a thickness of about 40 nm. This was too thin to measure any absorption but PL measurements showed an emission wavelength centered around 1440 nm, a substantial blue shift of the emission wavelength. SEM images revealed the NPs were packed closely together in the PMMA film but cracks were formed most likely due to rapid evaporation of toluene.

Drop casting of PbS was performed with and without PMMA. The case without PMMA showed an emission wavelength centered at 1600 nm while the case with PMMA had its emissions red shifted to 1650 nm. This points towards that the PMMA affects the NPs by lowering the energy levels of the NPs.

Spin coated samples were then made with a much higher PMMA to PbS ratio of 10:1 in an attempt to increase the thickness of the deposited film. The maximum spin speed was varied with the effect that the surface roughness decreased as the sin speed was increased. Absorption measurements showed an increased absorption cross section of $7.1 \cdot 10^{-15}$ cm^2 at 1500 nm for the NPs in the PMMA film compared to in the toluene solution. PL measurements of these samples showed an emission wavelength close to 1600 nm, while a PLE

spectrum showed an increase in the emission towards higher excitation wavelengths.

Quantum efficiency (QE) measurements were made on PbS NPs deposited in PMMA on silicon substrates yielding an internal QE in the order of 10^{-4}. The low QE is most likely caused by degradation of the organic passivation that has been reported to be unstable. The QE of the NPs still in the toluene solution was not possible to measure using the same method as for the thin films. This should however be done in some way before further work is done with the PbS NPs, to determine whether their QE always was that low, or if it is a result of the handling of the NPs during deposition and characterisation.

Besides the QE, the NPs showed promising optical properties, with emission wavelength near the erbium absorption. An increased absorption when deposited in the PMMA film. If the QE can be raised by proper surface passivation, and films with a higher thickness can be made so it absorbs a higher percentage of the incident light, there could be potential use for PbS NPs in a downshifting layer.

Part I

APPENDIX

A

MONOCHROMATOR MANUAL

The following is meant as a quick guide to use the Triax 180 monochromator. This will go over the labview driver that is used to control the monochromator and attached filter wheel.

First a quick overview of the files related to the monochromator is shown in Figure 42.

There is two pdf files, the first one is a control manual supplement which goes into detail about every sub-VI contained in the driver, and the second one called 'Spectrometer Control' is about the different communication interfaces. It goes through both RS-232 and IEEE 488 communication with a computer, describing the commands and their syntax. To simply use the monochromator these details about the communication is not needed since it is already programmed in the driver.

The three labview files are what will be used to control the monochromator. The *Isa_comm* and *ISA_UTL2* files contain low level VIs that control the communication between the computer and the monochromator. In this case the monochromator is connected using IEEE 488 (GPIB) interface. No changes should be made to these VIs and they will not be described further.

The *Isa_user* library is the one we are concerned with here, and contains all the user interface VIs needed to control the monochromator. An overview of the VIs contained in it is shown in Figure 43, and the ones marked with a green circle are the ones needed for control of the monochromator, the rest are either VIs for single channel data acquisition that only works with a separate controller, or demo VIs.

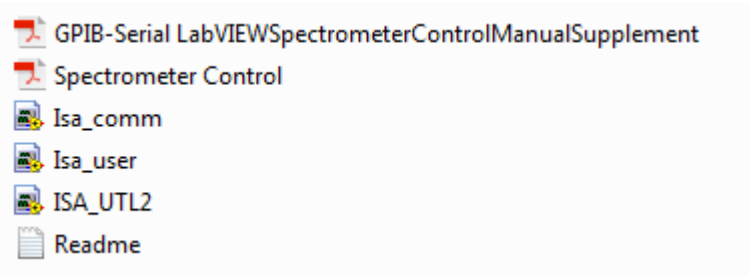

Figure 42: File overview.

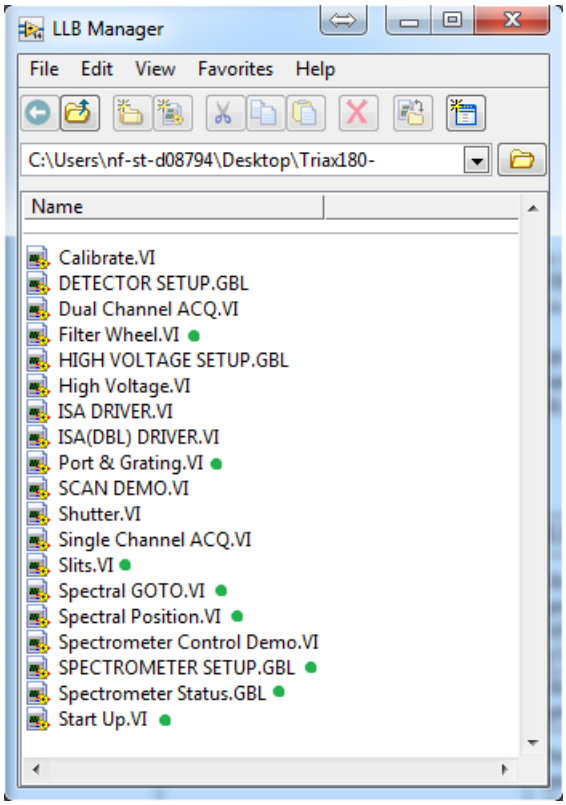

Figure 43: VIs contained in the Isa_user library.

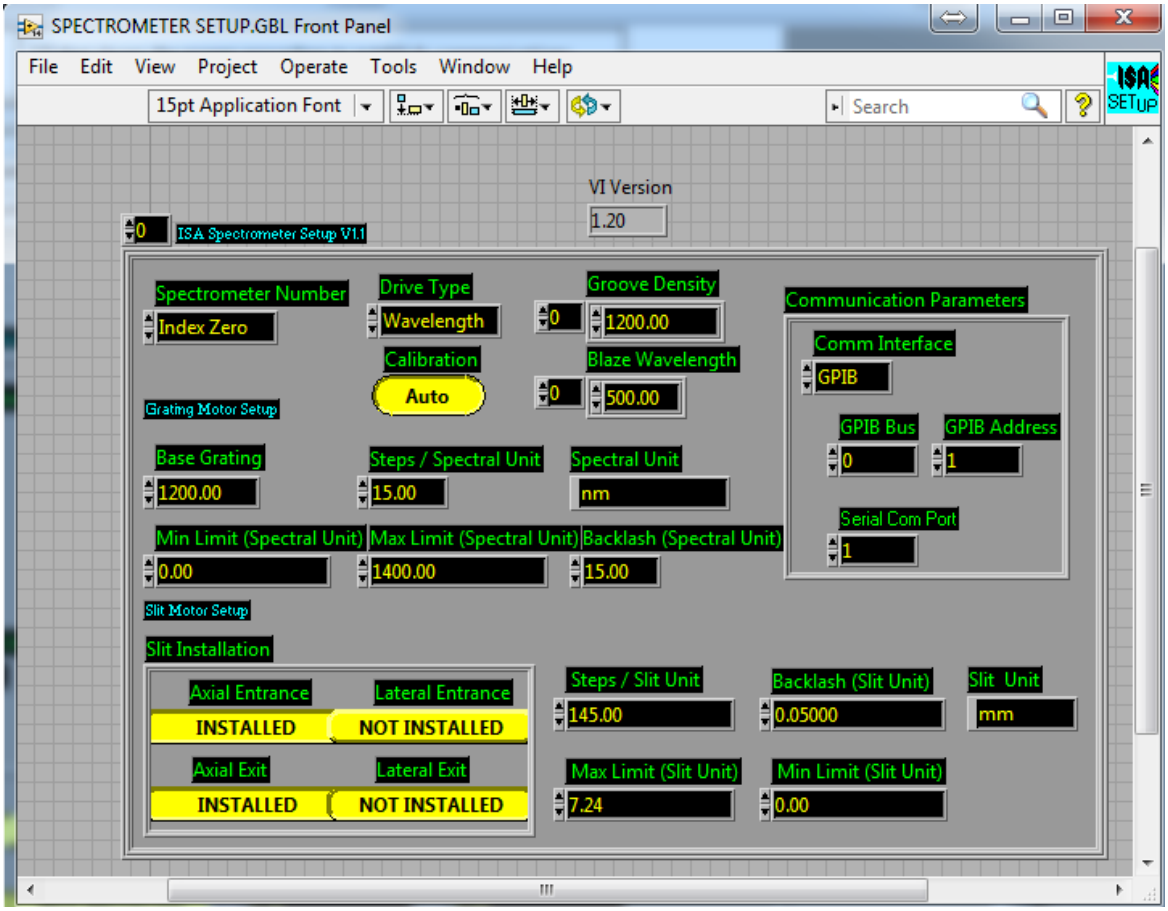

Figure 44: SPECTROMETER SETUP.GBL

SPECTROMETER SETUP.GBL

Is shown in Figure 44. This VI contain global parameters used by other VIs.

The *Spectrometer Number* is used to index different spectrometer if more are connected. Here we only have one, and the default number is zero.

Calibration can toggle between AUTO and MANUAL. This should be left at AUTO since the Triax series monochromators have automatic calibration.

Groove Density and *Blaze Wavelength* is parameters of the installed gratings. There are three grating installed on this one. Grating number 0, has a Groove Density of 1200 and Blaze Wavelength of 500 nm, Grating 1 has a Groove Density of 300 and a Blaze Wavelength of 2000 nm, Grating 2 has a Groove Density of 100 and a Blaze Wavelength of 3000 nm. This info can also be found on the side of the monochro-

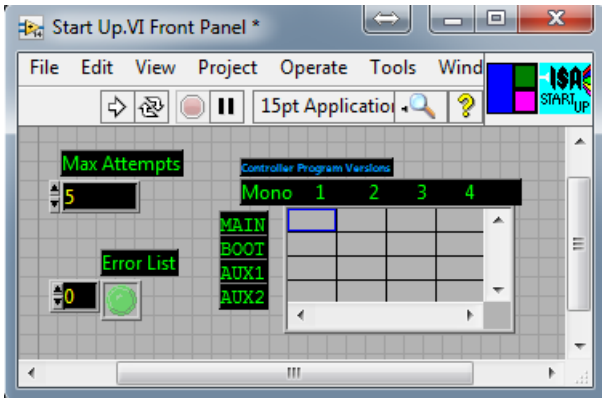

Figure 45: Start Up.VI

mator itself.

Drive Type indicate which motor driver is needed. For Triax monochromators this should be set to Wavelength.

The parameters for the *Grating Motor Setup* is specific to each type of monochromator, and should be left as is.

Slit Motor Setup is parameters for the installed slits. In this case the axial entrance and exit is installed. Slit limits are put in here. This limits the movement of the slits when using the Slit.VI to control the slit opening.

Communication Parameters specifies the communication parameters used by LabVIEW to communicate with the monochromator. The current set up uses GPIB with the shown adress and bus.

Start Up.VI

Shown in Figure 45. This VI must be run every time the computer or monochromator is powered on to establish communication and allow for the other VIs to communicate. The *Max Attempts* is the limit on how many times it will try to establish a connection before returning an error, which will be indicated by the Error LED.

Spectral GOTO.VI

Shown in Figure 46. This VI is used to control the wavelength of the light coming from the monochromator. The desired wavelength is entered in the *Target Position* field and when the VI is run, the monochromator will adjust the emission wavelength. The LEDs are: *Error* which lights up if the VI can not reposition the monochromator

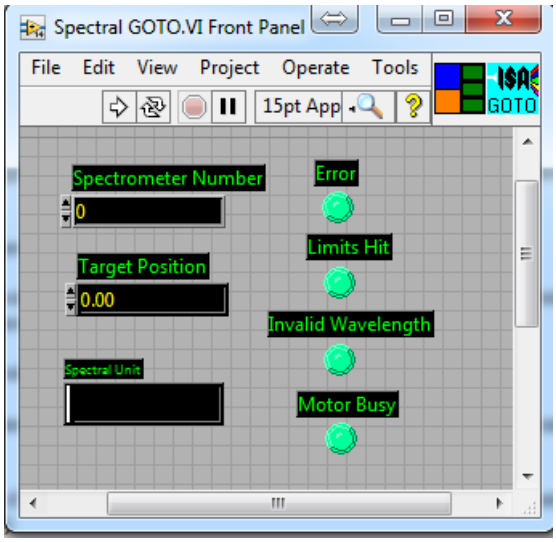

Figure 46: Spectral GOTO.VI

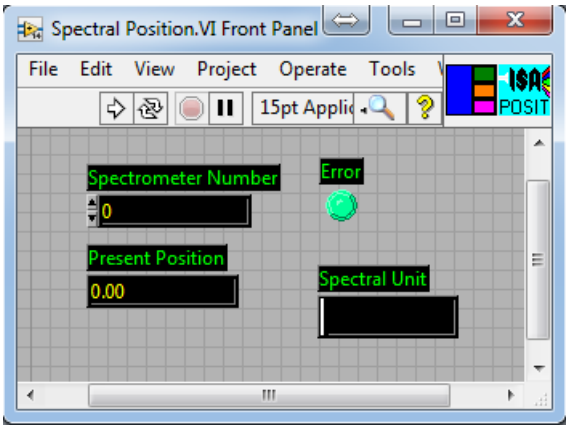

Figure 47: Spectral Position.VI

drive as requsted, *Limits Hit* which lights up if the grating travels to an extreme position (measured by a limit switch), *Invalid Wavelength* will light up if the target position is outside the limits specified in the SPECTROMETER SETUP.GBL file, and *Motor Busy* lights up as long as the motor is repositioning the grating.

Spectral Position.VI

Shown in Figure 47. This VI will return the current position of the grating when run, along with the spectral unit.

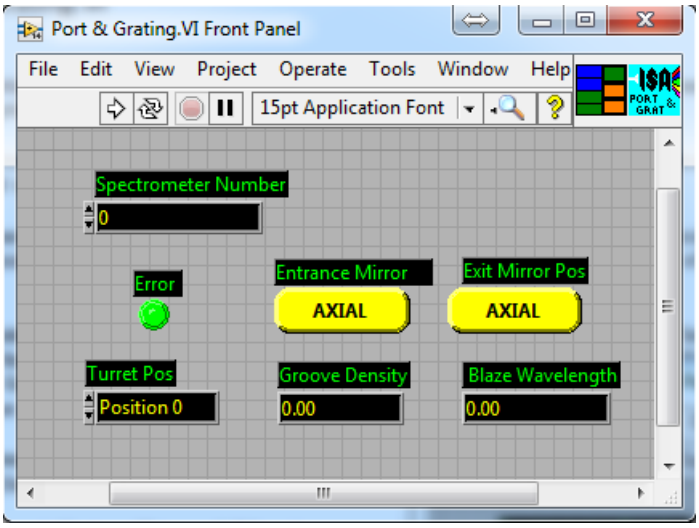

Figure 48: Port and Grating.VI

Port and Grating.VI

Shown in Figure 48. This VI will control the turret position, allowing the switch between the different installed gratings. The Groove Density and Blaze Wavelength fields are output and will return the values of the grating in the selected turret position.

Spectrometer Status.GBL

Shown in Figure 49. This will show the current positions of automated spectrometer accessories.

Slits.VI

Shown in Figure 50. This VI is used to control the slit width. Enter the desired values in the Axial Entrance and the Axial Exit fields.

Filter Wheel.VI

Shown in Figure 51. This is used to control to attached filter wheel. Filter wheel target position 1 is an empty slot with no filter, position 2 is an 800 nm long pass filter, and position 3 is a 1700 nm long pass filter.

A.1 USING THE MONOCHROMATOR

Normally the monochromator should be ready to use right away unless the computer or monochromator has been powered off since last

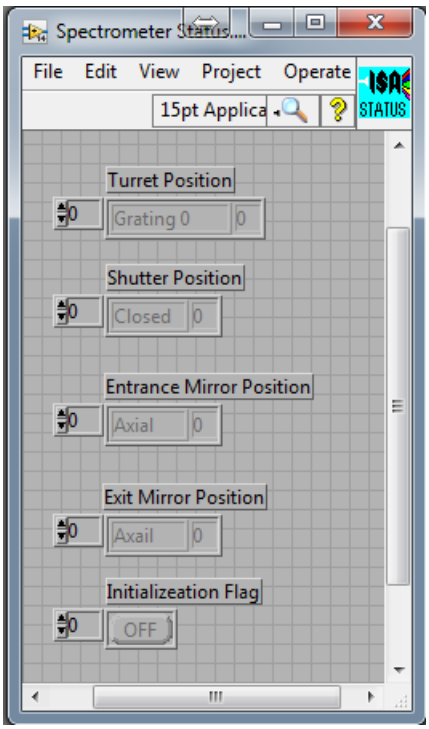

Figure 49: Spectrometer Status.GBL

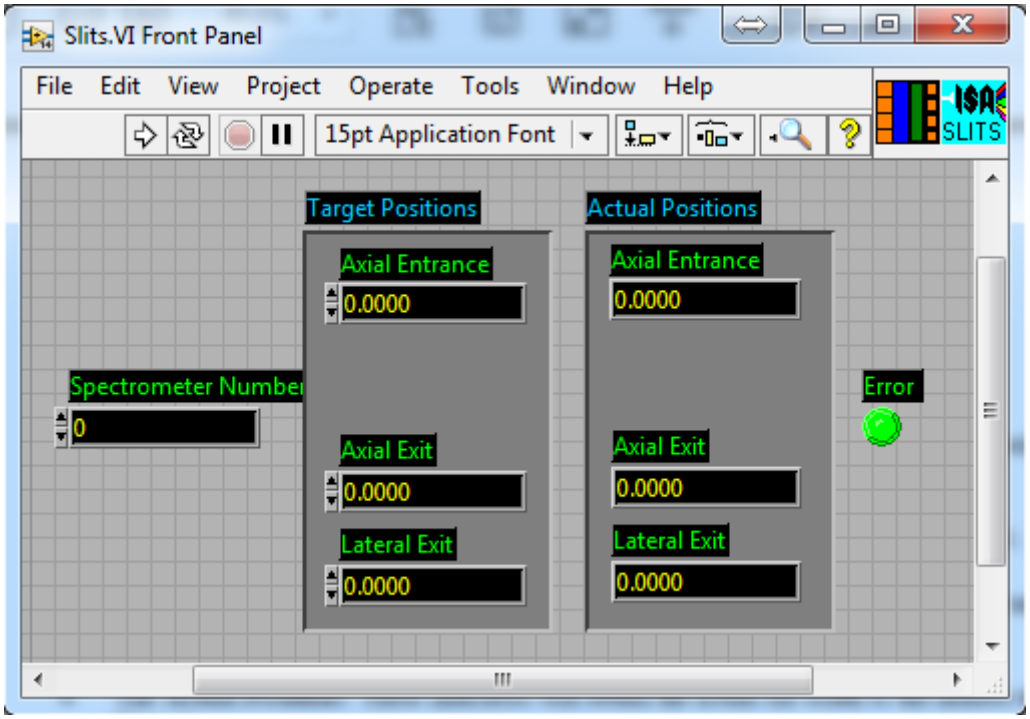

Figure 50: Slits.VI

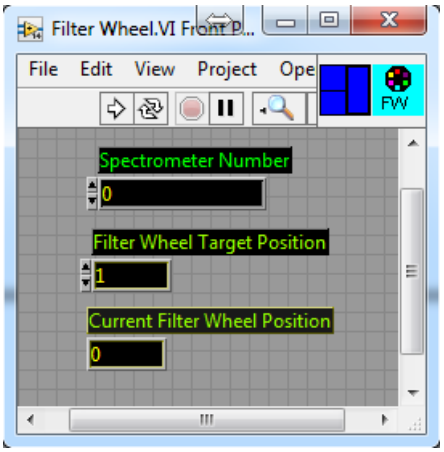

Figure 51: Filter Wheel.VI

use, in that case run the Start Up.VI to establish the connection. My experience in using the monochromator consisted in only really using the *Spectral Position.VI* and the *Filter Wheel.VI*. The slits was not used at all, just left open. When they are completely closed they still let some light out, which means when taking background spectra you will still need to block the exit in another way. Both the computer and monochromator was never turned off, so the monochromator was always ready to use without any initialisation, which made it very simple to just come down in the lab, turn on the lamp and it was ready.

BIBLIOGRAPHY

[1] [image] http://www.mse.iastate.edu/research/laboratories/sem/microscopy/how-does-the-sem-work/high-school/how-the-sem-works/.

[2] L. Cademartiri, E. Montanari, G. Calestani, A. Migilori, A. Guagliardi, and G. A. Ozin. "Size-Dependent Extinction Coefficients of PbS Quantum Dots". In: *J. AM. CHEM. SOC.* (2006).

[3] J Chang and E. R. Waclawik. "Colloidal semocinductor nanocrystals: controlled synthesis and surface chemistry in organic media". In: *The Royal Society of Chemistry* 4 (2014), pp. 23505–23527.

[4] O. Chen et al. "Compact high-quality CdSe-CdS core-shell nanocrystals with narrow emission linewidths and supressed blinking." In: *Nature Materials* 12 (2013), pp. 445–451.

[5] J. C. Goldschmidt, P. Löper, S. Fischer, S. Janz, M. Peters, S. W. Glunz, G. Willeke, E. Lifshitz, K. Krämer, and D. Biner. "Advanced Upconverter Systems with Spectral and Geometric Concentration for high Upconversion Efficiencies". In: *COMMAD* (2008), pp. 307–311.

[6] J. C. Goldschmidt, M. Peters, F. Dimroth, S. W. Glunz, and G. Willeke. "Efficicney Enhance of Fluorescent Concentrators with Photonic Structures and Material Combinations". In: *23rd European Photovoltaic Solar Energy Conference, 1-5 September, Valencia* (2008). DOI: 10.4229/23rdEUPVSEC2008-1CO.3.5.

[7] J. I. Goldstein, D. E. Newbury, P. Echlin, D. C. Joy, C. E. Lyman, E. Lifshin, L. Sawyer, and J. R. Michael. *Scanning Electron Miscroscopy and X-ray Microanalysis*. Plenum Press, New York, 1981.

[8] A. B. Greytak, P. M. Allen, W. Liu, J. Zhao, E. R. Young, Z. Popovic, B. J. Walker, D. G. Nocera, and M. G. Bawendi. "Alternating layer addition approach to CdSe/CdS core/shell quantum dots with near unity quantum yield and high on-time fractions." In: *Chem. Sci.* 3 (2012), pp. 2028–2034.

[9] M. A. Hines and G. D. Scholes. "Colloidal PbS Nanocrystals with Size-Tunable Near-Infrared Emission: Obervation of Post-Synthesis Self-Narrowing of the Particle Size Distribution". In: *Adv. Mater* 15 (2003), pp. 1844–1849.

[10] International Energy Agency (IEA). *Technology Roadmap: Solar Photovoltaic Energy - 2014 Edition*. http://www.iea.org/publications/freepublications/publication/TechnologyRoadmapSolarPhotovoltaicEnergy_2014edition.pdf. 2014.

[11] S. Kalytchuk et al. “Semiconductor Nanocrystals as Luminescent Down-Shifting Layers To Enhance the Efficiency of Thin-Film CdTe/CdS and Crystalline Si Solar Cells”. In: *J. Phys. Chem.* 118 (2014), pp. 16393–16400.

[12] I. Kang and F. W. Wise. “Electronic structure and optical properties of PbS and PbSe quantum dots”. In: *J. Opt. Soc. Am.* 14 (1997), pp. 1637–1646.

[13] I. Moreels, Y. Justo, B. D. Geyter, K. Haustraete, J. C. Martins, and Z. Hens. “Size-Tunable, Bright, and Stable PbS Quantum Dots: A Surface Chemistry Study”. In: *ASC Nano* 5 (2011), pp. 2004–2012.

[14] Michael W. Murphy. *spin-coating*. [image] http://www.spincoater.com/what-is-spin-coating.php.

[15] Z. Ning, Y. Ren, S. Hoogland, O. Voznyy, L. Levina, P. Stadler, X. Lan, D. Zhitomirsky, and E. H. Sargent. “All-Inorganic Colloidal Quantum Dot Photovoltaics Employing Solution-Phase Halide Passivation”. In: *Advanced Materials* 24 (2012), pp. 6295–6299.

[16] X. Pi, Q. Li, D. Li, and D. Yang. “Spin-coating silicon quantum-dot ink to improve solar cell efficiency”. In: *Solar Energy Materials and Solar Cells* 95 (2011), pp. 2941–2945.

[17] P. Reiss, M. Protière, and L. Li. “Core/Shell Semiconductor Nanocrystals”. In: *Small* 5 (2009), pp. 154–168.

[18] B. S. Richards. “Enhancing the performance of silicon solar cells via the application of passive luminescence conversion layers”. In: *Solar Energy Materials and Solar Cells* 90 (2006), pp. 2329–2337.

[19] R. Rothermund, S. Kreuzer, T. Umundum, G. Meinhardt, T. Fromherz, and W. Jantsch. “External quantum efficiency analysis of Si solar cells with II-VI nanocrystal luminescent down-shifting layers”. In: *Energy Procedia* 10 (2011), pp. 83–87.

[20] Edward H. Sargent. “Infrared Quantum Dots”. In: *Adv. Mater* 17 (2005), pp. 515–522.

[21] W. G. J. H. M. van Sark, A. Meijerink, and R. E. I. Schropp. “Solar Spectrum Conversion for Photovoltaics Using Nanoparticles”. In: *Third Generation Photovoltaics* (2012). Editor: V. Fthenakis, InTech.

[22] W. Shockley and H. J. Qeuisser. “Detailed Balance Limit of Efficiency of p-n Junction Solar Cells”. In: *Journal of Applied Physics* 31 (1961), pp. 510–519.

[23] J. Tang et al. “Colloidal-quantum-dot photovoltaics using atomic-ligand passivation”. In: *Nature materials* 10 (2011), pp. 765–771.

[24] T. Trupke, A. Shalav, B. S. Richards, P. Würfel, and M. A. Green. "Efficiency enhancement of solar cells by luminescent upconversion of sunlight". In: *Solar Energy Materials and Solar Cells* 90 (2006), pp. 3327–3338.

[25] Y. Wang, A. Suna, W. Mahler, and R. Kasowski. "PbS in polymers. From molecules to bulk solids". In: *J. Chem. Phys.* 87 (1987), pp. 7315–7322.

[26] F. W. Wise. "Lead Salt Quantum Dots: the limit of Strong Quantum Confinement". In: *Acc. Chem. Res.* 33 (2000), pp. 773–780.

[27] B. Zhang, G. Li, J. Zhang, Y. Zhang, and L. Zhang. "Synthesis and characterisation of PbS nanocrystals in water/$C_{12}E_9$/cyclohexane microemulsions". In: *Nanotechnology* 14 (2003), pp. 443–446.

[28] D. Zherebetskyy, M. Scheele, Y. Zhang, N. Bronstein, C. Thompson, D. Britt, M. Salmeron, P. Alivisatos, and L. Wang. "Hydroxylation of the surface of PbS nanocrystals passivated with oleic acid". In: *Science* 344 (2014), pp. 1380–1384.